AD-A045 307 ARMY ELECTRONICS COMMAND FORT MONMOUTH N J F/G 9/1

FORCE-FREQUENCY AND OTHER EFFECTS IN DOUBLY ROTATED VIBRATORS.(U)

SEP 77 A BALLATO, T LUKASZEK, E P EERNISSE

UNCLASSIFIED ECOM-4536 NL

|OF|

AD
A045307

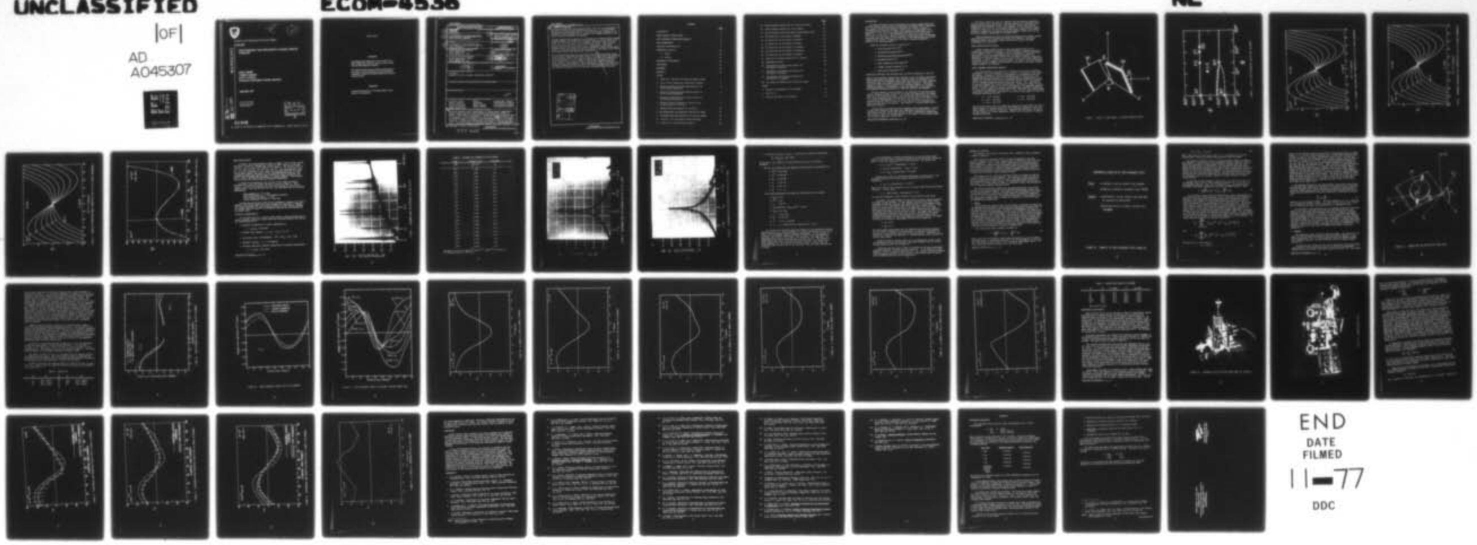

END
DATE
FILMED
11-77
DDC

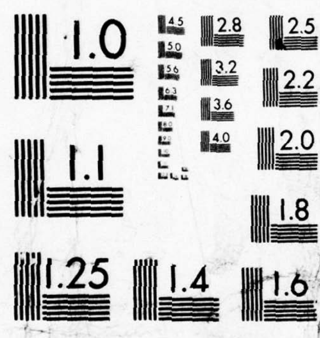


MICROCOPY RESOLUTION TEST CHART
NATIONAL BUREAU OF STANDARDS-1963-A

(12)

Research and Development Technical Report

ECOM-4536

AD A045307

# FORCE-FREQUENCY AND OTHER EFFECTS IN DOUBLY ROTATED VIBRATORS

Arthur Ballato
Theodore Lukaszek
Errol P. EerNisse
Electronics Technology & Devices Laboratory

September 1977



DISTRIBUTION STATEMENT

Approved for public release; distribution unlimited.



ECOM

US ARMY ELECTRONICS COMMAND FORT MONMOUTH, NEW JERSEY 07703

# NOTICES

## Disclaimers

The findings in this report are not to be construed as an official Department of the Army position, unless so designated by other authorized documents.

The citation of trade names and names of manufacturers in this report is not to be construed as official Government indorsement or approval of commercial products or services referenced herein.

## Disposition

Destroy this report when it is no longer needed. Do not return it to the originator.

UNCLASSIFIED

SECURITY CLASSIFICATION OF THIS PAGE (When Data Entered)

## REPORT DOCUMENTATION PAGE

READ INSTRUCTIONS BEFORE COMPLETING FORM

1. REPORT NUMBER: 14 ECOM-4536
2. GOVT ACCESSION NO.
3. RECIPIENT'S CATALOG NUMBER
4. TITLE (and Subtitle): 6 FORCE-FREQUENCY AND OTHER EFFECTS IN DOUBLY ROTATED VIBRATORS.
5. TYPE OF REPORT & PERIOD COVERED: 9 Research and development Technical Report. for Aug 77,
6. PERFORMING ORG. REPORT NUMBER
7. AUTHOR(s): 10 Arthur Ballato, Theodore Lukaszek and Errol P. EerNisse
8. CONTRACT OR GRANT NUMBER(s): 17 09
9. PERFORMING ORGANIZATION NAME AND ADDRESS: US Army Electronics Command, ATTN: DRSEL-TL-ML, Fort Monmouth, NJ 07703
10. PROGRAM ELEMENT, PROJECT, TASK AREA & WORK UNIT NUMBERS: 16 1T1 61101 A 91A 09 455
11. CONTROLLING OFFICE NAME AND ADDRESS: US Army Electronics Command, ATTN: DRSEL-TL-ML, Fort Monmouth, NJ 07703
12. REPORT DATE: 11 Sep[redacted]77
13. NUMBER OF PAGES: 45
14. MONITORING AGENCY NAME & ADDRESS (if different from Controlling Office): 12 50p.
15. SECURITY CLASS. (of this report): UNCLASSIFIED
15a. DECLASSIFICATION/DOWNGRADING SCHEDULE

16. DISTRIBUTION STATEMENT (of this Report)

Statement A.
Approved for public release; distribution unlimited.

17. DISTRIBUTION STATEMENT (of the abstract entered in Block 20, if different from Report)

18. SUPPLEMENTARY NOTES

omega L

19. KEY WORDS (Continue on reverse side if necessary and identify by block number)

| | | |
|---|---|---|
| Frequency control | Quartz | Piezoelectric crystals |
| Crystal resonators | Transducers | Piezoelectric vibrators |
| Crystal oscillators | Filter crystals | Force-frequency effects |
| Shock and vibration | Energy trapping | Acceleration resistance |
| Doubly rotated cuts | | |

20. ABSTRACT (Continue on reverse side if necessary and identify by block number)

Precision frequency control requirements for future digital communication systems require improved crystal resonator performance in a number of aspects. Accordingly, the potential of doubly rotated quartz cuts has begun to be explored. In the neighborhood of the SC-cut (YXwl) phi/theta, phi approximately equals 21.9 degrees, theta approximately equals +33.9 degrees, a variety of effects having their bases in nonlinear elasticity have been shown, or are predicted, to be improved with respect to corresponding AT-cut values. The static frequency-temperature behavior also shows improvement.

DD FORM 1 JAN 73 1473 EDITION OF 1 NOV 65 IS OBSOLETE

UNCLASSIFIED

SECURITY CLASSIFICATION OF THIS PAGE (When Data Entered)

037 620

4B

20. ABSTRACT (continued)

This report concerns the force-frequency effect, thus far not investigated in any detail for doubly rotated quartz plate vibrators. It relates initial stress produced by mounting supports to resonance frequency changes; it contributes to long-term aging, and is related to the frequency excursions produced in shock and vibration environments.

In-plane diametric forces applied to the periphery of vibrating plates produce frequency changes that depend upon the azimuth angle psi in the plane of the plate. For the IT-cut at phi = 19.1 degrees, the maximum value was found previously to be only about one-third that of the AT-cut. This points to a reduced coefficient at the SC-cut as well. Measurements of the force-frequency effect coefficients have now been extended to doubly rotated quartz plates. Also given are charts of the mode spectra in the region of the thickness modes, and the modal temperature coefficients.

The force-coefficient data are compared with theoretically predicted values obtained from a variational principle applied to an anisotropic disc supported at two diametric points. This analysis departs from previous treatments in two major respects: 1) the isotropic stress pattern is replaced by anisotropic stress; 2) the elastic problem is treated for triclinic symmetry, rather than monoclinic symmetry. These investigations verify the superiority of doubly rotated plates with respect to the force-frequency effect and provide further motivation for their continued development and utilization.

CONTENTS

Page



TABLES

## INTRODUCTION

Precision frequency control requirements for digital communication and position location systems currently undergoing development make it imperative that crystal resonator performance be improved in a number of aspects. Accordingly, the potential of doubly rotated quartz cuts has begun to be explored.[1-13]* For cuts on the upper zero temperature coefficient locus in general ($\theta \approx +34°$), and in the neighborhood of the SC-cut in particular ($\phi \approx 21.9°$, $\theta \approx +33.9°$), a variety of effects having their bases in nonlinear elasticity have been shown, or are predicted, to be reduced below the corresponding AT-cut values. In addition, the static frequency-temperature behavior shows some improvement.

Among the nonlinear effects of interest are:

- Force-frequency[1,11,13-25]*
- Acceleration-frequency[26,27]*
- Resonance amplitude-frequency[10,28-31]*
- Intermodulation[32-35]*
- Mode coupling-activity dips[36-43]*
- Dynamic thermal-frequency[2,4,7-9]
- Film stress-frequency[3,5,44]*

Additional references and discussion may be found in References 6 and 45.*

Some of these nonlinear effects have received, or are receiving, theoretical and/or experimental treatments; this technical report is principally concerned with the force-frequency effect which has thus far not been investigated in any detail for doubly rotated quartz plate vibrators. This effect relates the initial stress produced by the mounting supports to resonance frequency changes; it contributes to long-term aging and is also related to the frequency excursions produced in shock and vibration environments.

In-plane diametric forces applied to the periphery of vibrating plates produce frequency changes (order $10^{-7}$ per gram) that depend upon the azimuth angle $\psi$ in the plane of the plate. If $\psi$ is measured from the $X_1''$ axis, then it is found experimentally[1,11,14-18,20] that for the AT-cut the effect is zero at $\psi$ values of approximately 60° and 120°. For the IT-cut at $\phi = 19.1°$, Ballato[1] found the zeros to occur at $\psi = 85°$ and 163° with a maximum value about one-third that of the AT-cut. This points to a reduced coefficient at the SC-cut as well.

In this report we extend the force-frequency effect measurement to doubly rotated quartz plates on the upper zero temperature coefficient locus, concentrating on the SC- and FC-cuts because of their technological significance. Also given are charts of the mode spectra in the region of the thickness modes and the modal temperature coefficients.

---

*See list of references beginning on p. 39.

The force coefficient data are compared with theoretically predicted values obtained from a variational principle applied to an anisotropic disc supported at two diametric points. This analysis departs from previous treatments[3,5,19,21,23,24] in two major respects: 1) the isotropic stress pattern is replaced by the more accurate anisotropic stress; 2) the elastic problem is treated for the general triclinic symmetry, rather than for the monoclinic symmetry appropriate to rotated-Y-cuts.

These investigations verify the predicted superiority of doubly rotated quartz plates over the conventional AT-cut, with respect to the force-frequency effect, and provide further motivation for their continued development and utilization.

## DOUBLY ROTATED CRYSTAL PLATES

Doubly rotated crystal plates are the most general kind of one-dimensional thickness-mode vibrator. The orientation is uniquely specified by two angles--$\phi$ and $\theta$. Following the usual convention,[46*] the orientation with respect to the crystallographic axes is described as $(YXw\ell)\phi/\theta$. Examples of singly and doubly rotated cuts are shown in Figure 1 along with the angles.[6] Shown in Figure 2 is the locus of zero first-order temperature coefficient (ZTC) for quartz resonator plates. In quartz, the first rotation lowers the apparent symmetry from trigonal to monoclinic; the second rotation further lowers it to triclinic.

## STATIC FREQUENCY-TEMPERATURE BEHAVIOR

For quartz plates on the upper ($\theta > 0$) ZTC locus, the static frequency-temperature (f-T) curve exhibits a cubic behavior. The AT-cut is the classical example. Whereas the inflection temperature (the temperature half way between turnover points) occurs at room temperature for the AT-cuts, this temperature increases steadily with increasing angle $\phi$, becoming 48°C at the FC-cut, 74°C at the IT-cut, 95°C at the SC-cut, and 157°C for the rotated-X-cut.[13] Frequency-temperature-angle curves for the AT- , FC- , and SC-cuts are given in Figures 3, 4, and 5, respectively. Typical f-T curves for the SC-cut are shown in Figure 6 for the c- and b-modes. Dots represent measured points. For the b-mode (the faster, quasi-shear mode, classed as undesired), the first-order temperature coefficient is $-25.1 \times 10^{-6}/K$. The c-mode (slower, quasi-shear, desired mode) curve was fit by quintic least-squares to yield the following coefficients at 25°C:

$a = 0.38 \times 10^{-6}/K$ $\quad$ $d = 136. \times 10^{-15}/K^4$

$b = -11.4 \times 10^{-9}/K^2$ $\quad$ $e = 175. \times 10^{-18}/K^5$

$c = 26.8 \times 10^{-12}/K^3$

The SC-cut is seen to have its inflection temperature around 100°C, so that it would normally be operated around its lower turnover temperature, where the upper turnover is used for the AT-cut. Compared with the AT-cut, the SC-cut is also flatter, so a given temperature control will correspond to a smaller frequency deviation.

---

*See list of references beginning on p. 39.

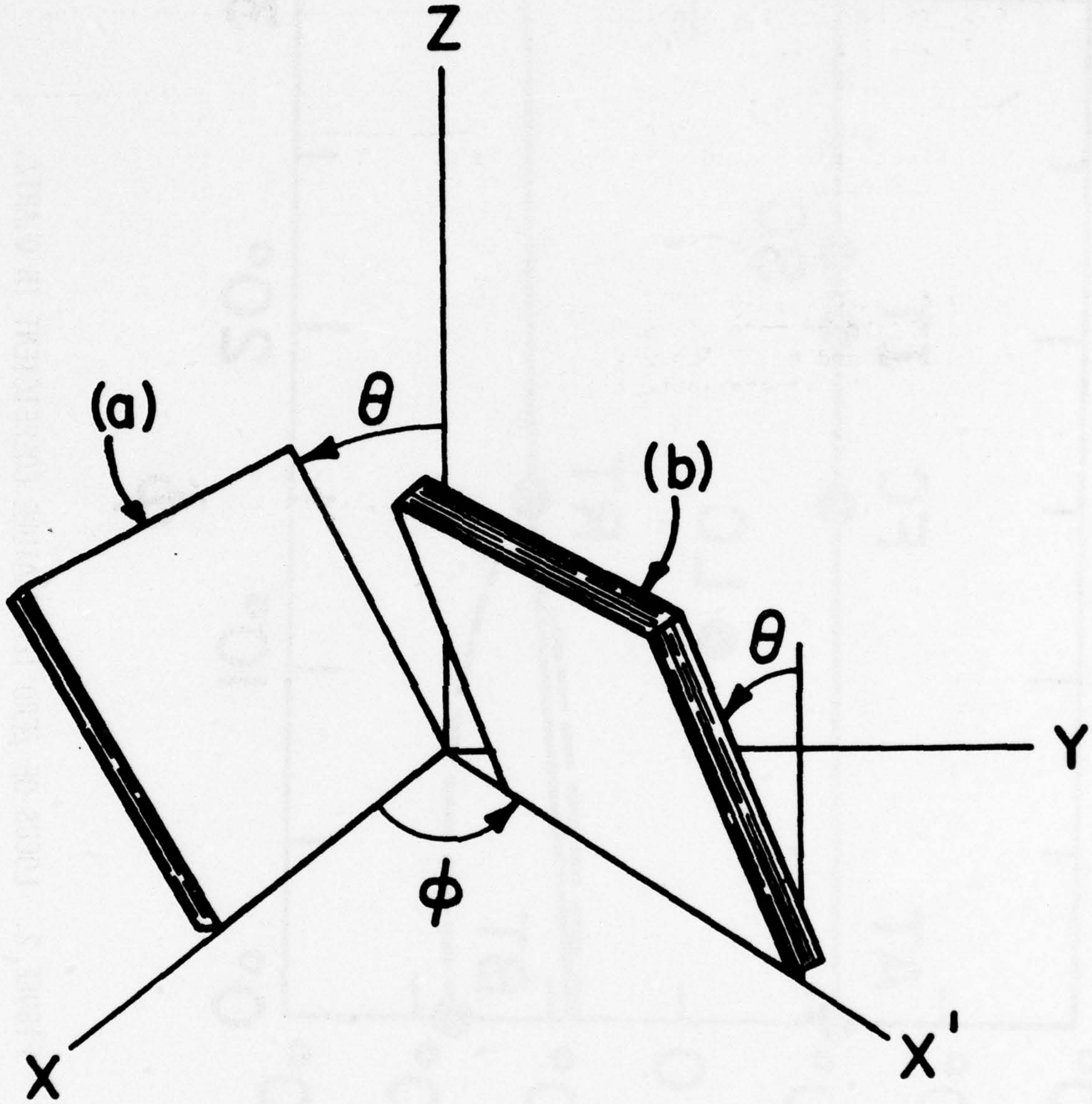


FIGURE 1. SINGLY (a) AND DOUBLY (b) ROTATED CRYSTAL PLATES.

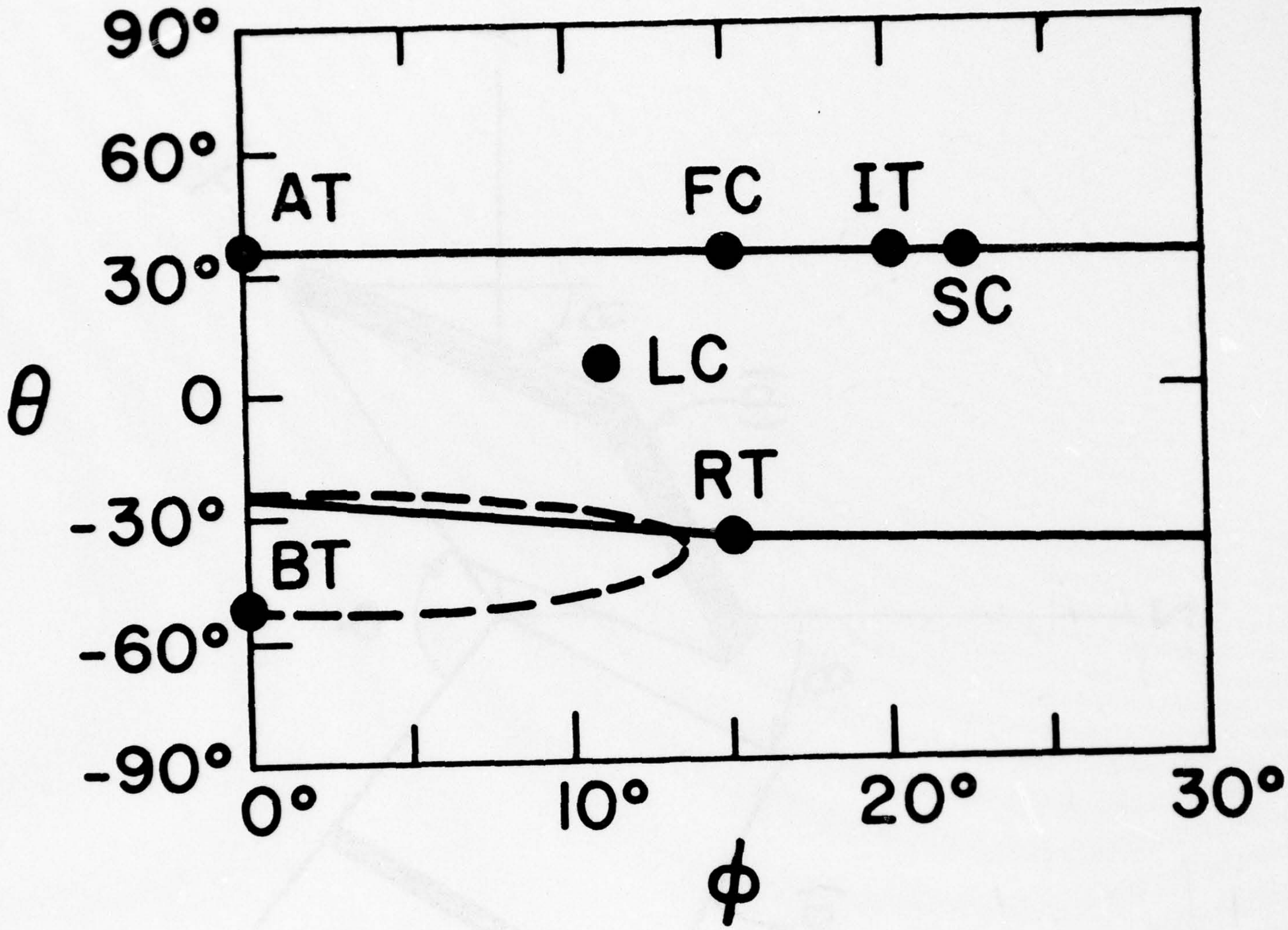


FIGURE 2. LOCUS OF ZERO TEMPERATURE COEFFICIENT IN QUARTZ.

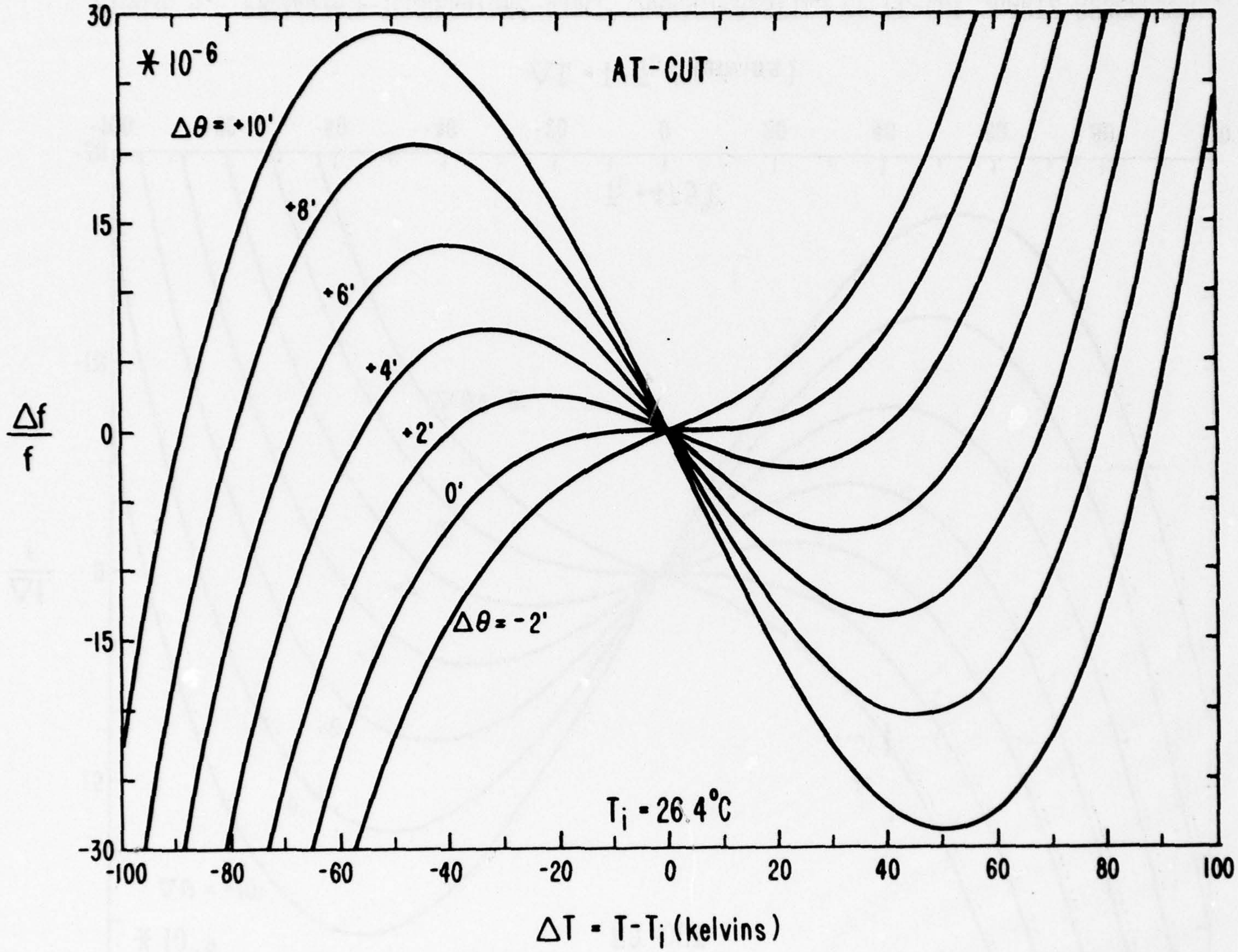


FIGURE 3. FREQUENCY-TEMPERATURE-ANGLE CHARACTERISTICS OF AT-CUT QUARTZ RESONATORS.

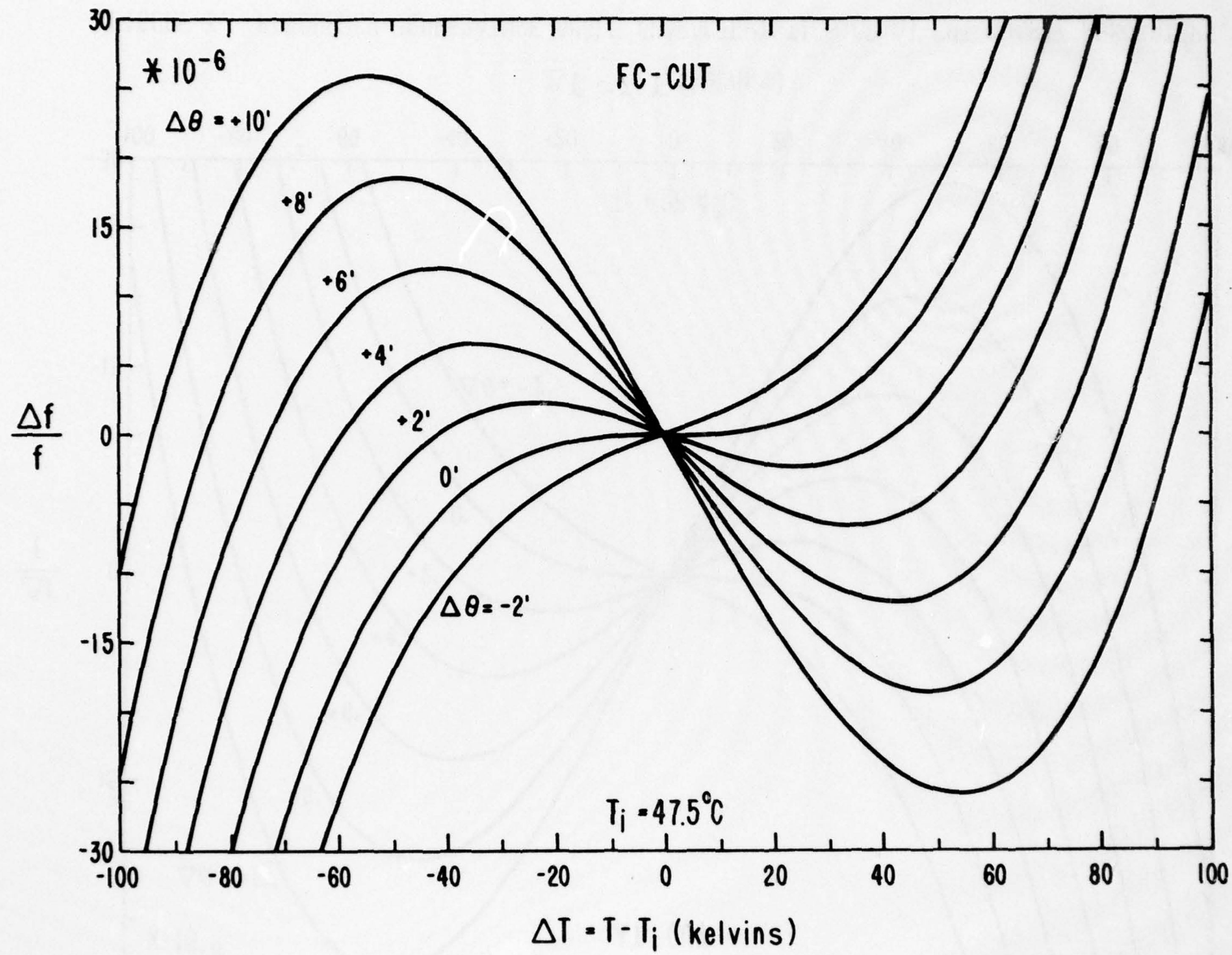


FIGURE 4. FREQUENCY-TEMPERATURE-ANGLE CHARACTERISTICS OF FC-CUT QUARTZ RESONATORS.

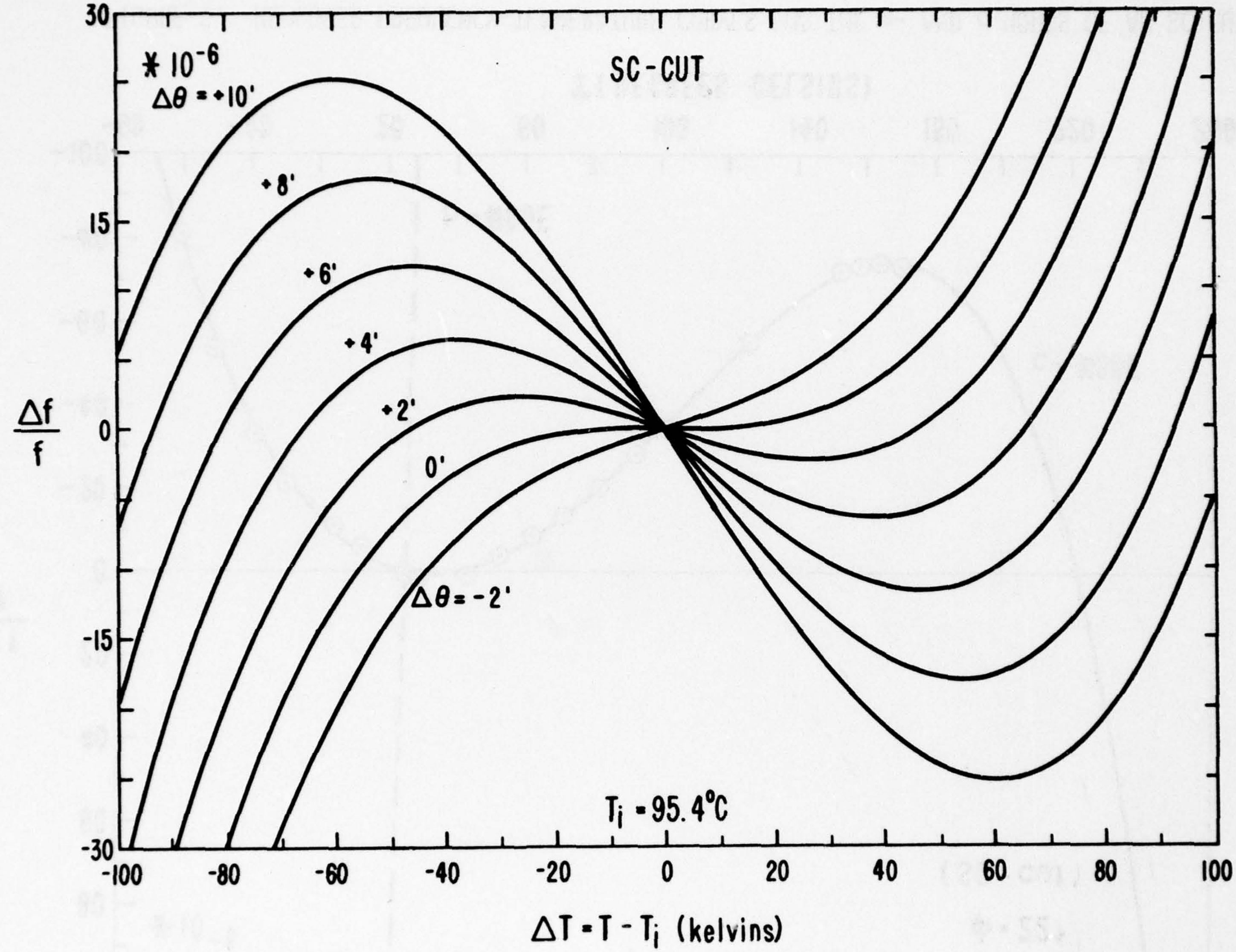


FIGURE 5. FREQUENCY-TEMPERATURE-ANGLE CHARACTERISTICS OF SC-CUT QUARTZ RESONATORS

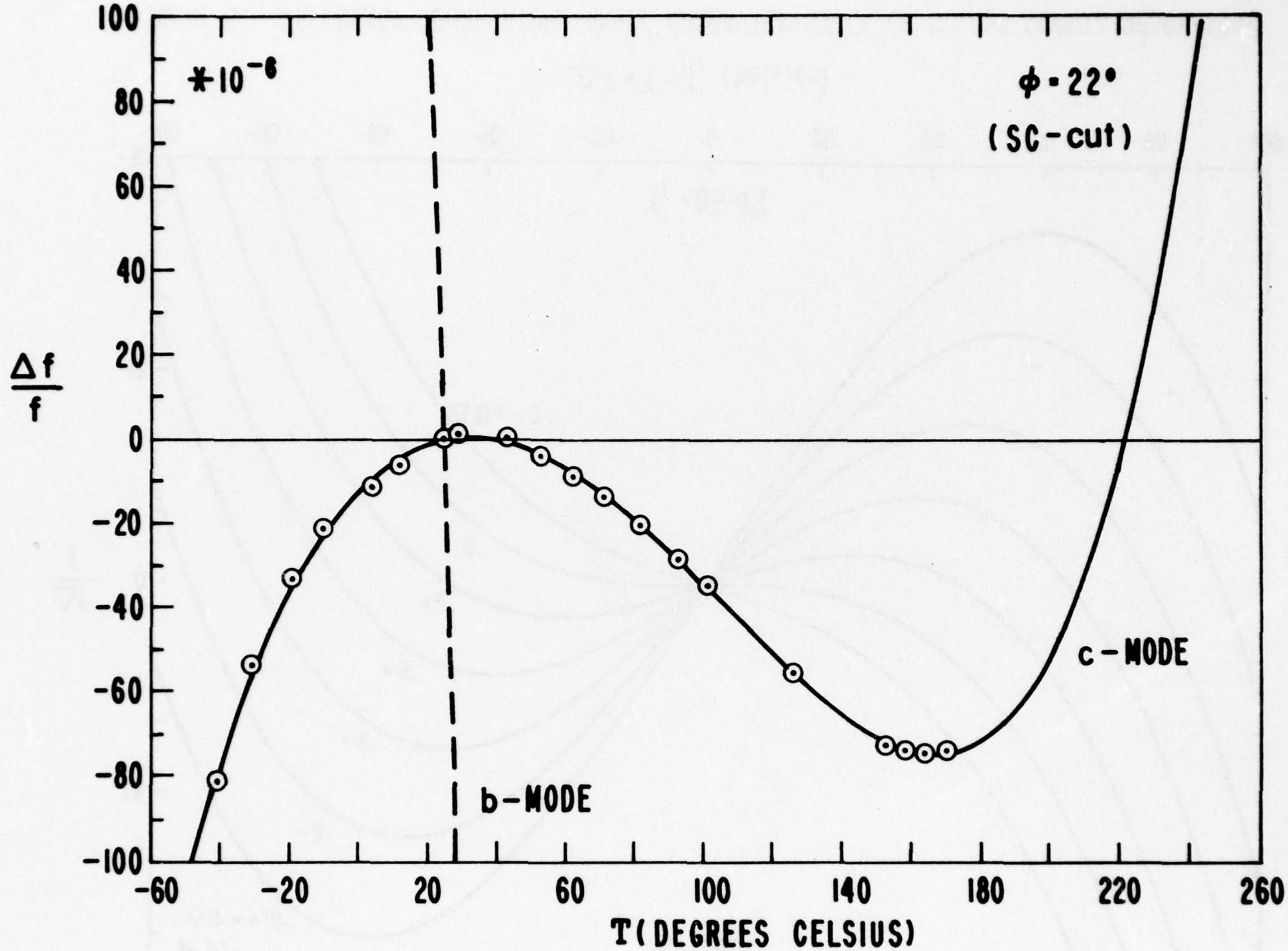


FIGURE 6. MEASURED FREQUENCY-TEMPERATURE CURVES FOR THE B- AND C-MODES OF AN SC-CUT.

MODE SPECTROGRAPHS[6]

A wideband mode spectrograph is shown in Figure 7 for an SC-cut crystal. The modes, in order of frequency, are denoted as $m^{(M)}$, where m is the mode type (a, b, or c) and M is the order of the harmonic. The sequence shown is $c_{\varsigma}^{(1)}$ $b_{\varsigma}^{(1)}$ $a_{\varsigma}^{(1)}$ $c_{\varsigma}^{(3)}$ $b_{\varsigma}^{(3)}$ $c_{\varsigma}^{(5)}$ $b_{\varsigma}^{(5)}$ $a_{\varsigma}^{(3)}$ and $c^{(7)}$. The thickness-shear mode $TS_1$ at cutoff corresponds to the c-mode; the thickness-twist $TT_1$ at cutoff corresponds to mode b, and mode a is the thickness-stretch mode, TE. The spacings and amplitudes measured agree closely with those calculated last year.[6] Table 1 extends the calculations to higher harmonics The ratios of frequencies are for unelectroded antiresonance frequencies.

In Figure 8 the spectrum in the vicinity of the c-mode is shown; a narrowband plot about the b-mode resonance is given in Figure 9. From Figures 7, 8, and 9 one sees how very clean the spectrum is, even for the harmonic modes. The flat SC-plate used for this experiment had the following measurements:

plate diameter $\Phi_a = 14.18$ mm;
electrode diameter $\Phi_e = 5.0$ mm (keyhole pattern);
mass loading (plateback) $\mu = 1.8\%$;
c-mode fundamental frequency = 5.937 MHz.

Although one would suspect that the SC orientation, because of its lower symmetry, would have a more complicated unwanted mode spectrum, it appears that energy trapping[47,48*] can be applied readily to these plates, although the optimum electrode shape[49*] and plateback relations are not available at the present time.

ELECTRICAL CHARACTERISTICS

For the ideal case of an infinite plate having a uniform distribution of motion laterally, the SC-cut c-mode yields the following physical and electrical characteristics[12,13]:

- Dielectric permittivity of static capacitance $C_o$:

  $$\varepsilon = C_o t_a / A_e = 39.8 \text{ pF/m}$$

- Motional time constant: $\tau_1 = R_1 C_1 = P_1 \Gamma_1 = 11.7$ fs

- Capacitance ratio of fundamental: $r^{(1)} = C_o/C_1 = \varepsilon/\Gamma_1 = 496$

- Frequency constant: $N = 1.797$ MHz-mm

- Motional capacitance constant (permittivity of motional capacitance):

  $$\Gamma_1 = C_1 t_a / A_e = 80.3 \text{ fF/m}$$

*See list of references on p. 42.

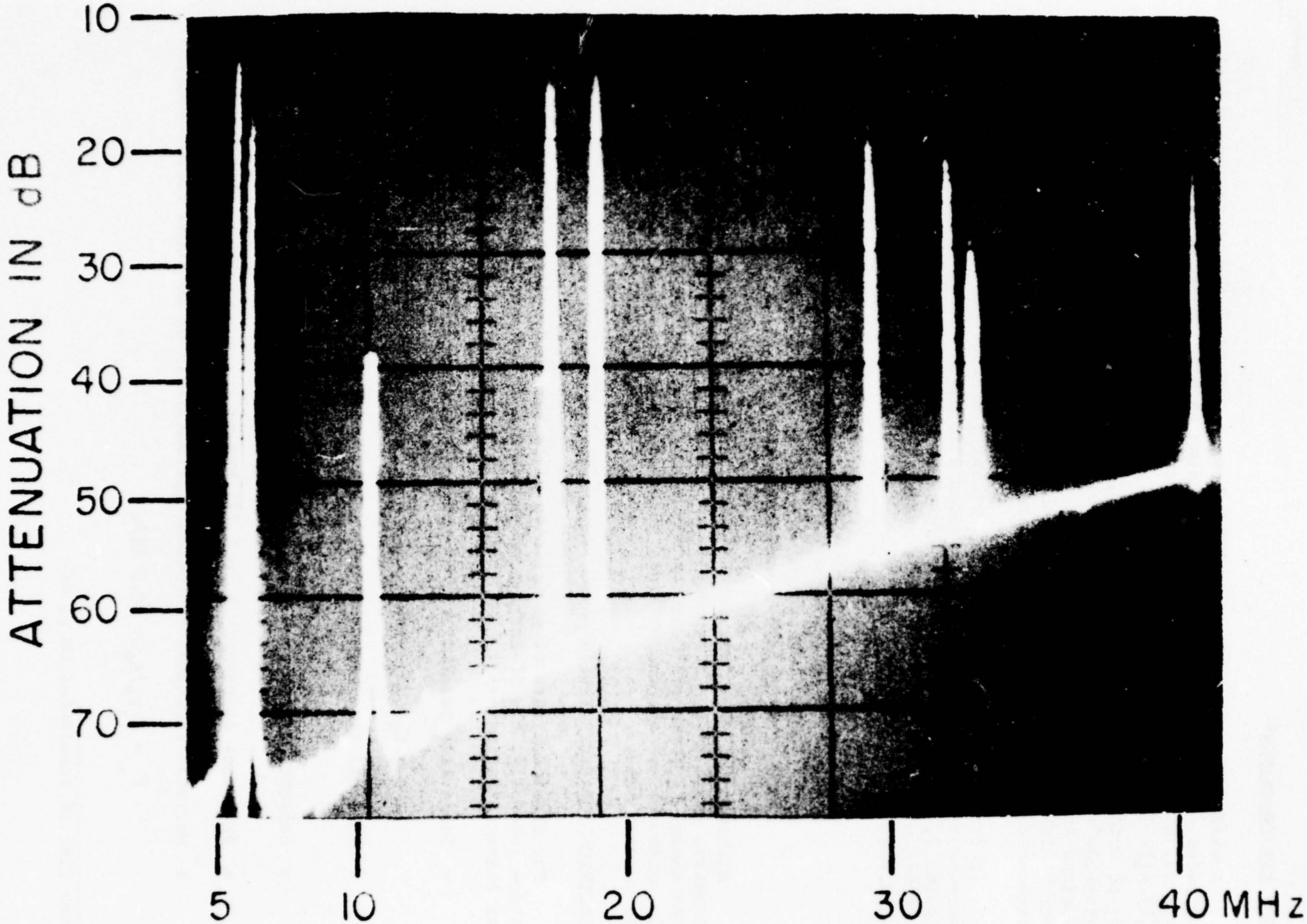


FIGURE 7. WIDEBAND MODE SPECTROGRAPH FOR THE SC-CUT.

TABLE 1. SEQUENCE AND STRENGTHS OF SC-CUT MODES.

| Mode | Frequency Ratio | Strength |
|---|---|---|
| $m^{(M)}$ | $f_m^{(M)}/f_c^{(1)}$ | dB |
| $c^{(1)}$ | 1.000 | 4.3 |
| $b^{(1)}$ | 1.100 | 0.0 |
| $a^{(1)}$ | 1.882 | 10.4 |
| $c^{(3)}$ | 3.000 | 23.4 |
| $b^{(3)}$ | 3.301 | 19.1 |
| $c^{(5)}$ | 5.000 | 32.3 |
| $b^{(5)}$ | 5.501 | 28.0 |
| $a^{(3)}$ | 5.646 | 29.5 |
| $c^{(7)}$ | 7.000 | 38.1 |
| $b^{(7)}$ | 7.701 | 33.8 |
| $c^{(9)}$ | 9.000 | 42.5 |
| $a^{(5)}$ | 9.410 | 38.3 |
| $b^{(9)}$ | 9.902 | 38.2 |
| $c^{(11)}$ | 11.000 | 46.0 |
| $b^{(11)}$ | 12.102 | 41.7 |
| $c^{(13)}$ | 13.000 | 48.9 |
| $a^{(7)}$ | 13.174 | 44.2 |
| $b^{(13)}$ | 14.302 | 44.6 |
| $c^{(15)}$ | 15.000 | 51.4 |
| $b^{(15)}$ | 16.503 | 47.0 |
| $a^{(9)}$ | 16.938 | 48.6 |
| $c^{(17)}$ | 17.000 | 53.5 |

(Strength = dB level of mode $m^{(M)}$ below $b^{(1)}$; mode $b^{(1)}$ (SC-cut) is 5.5 dB below mode $c^{(1)}$ (AT-cut).)

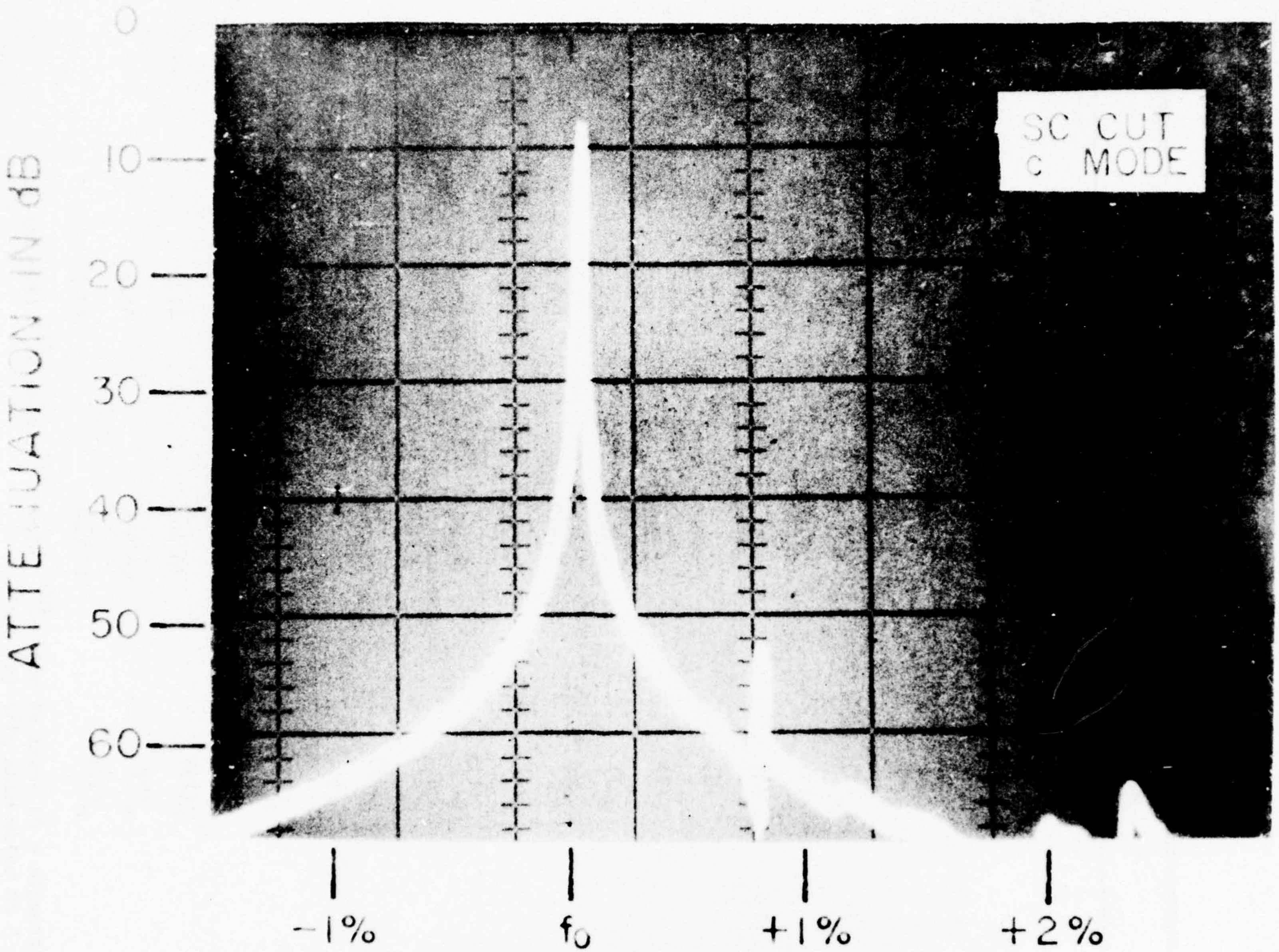


FIGURE 8. NARROWBAND MODE SPECTROGRAPH FOR THE SC-CUT c-MODE.

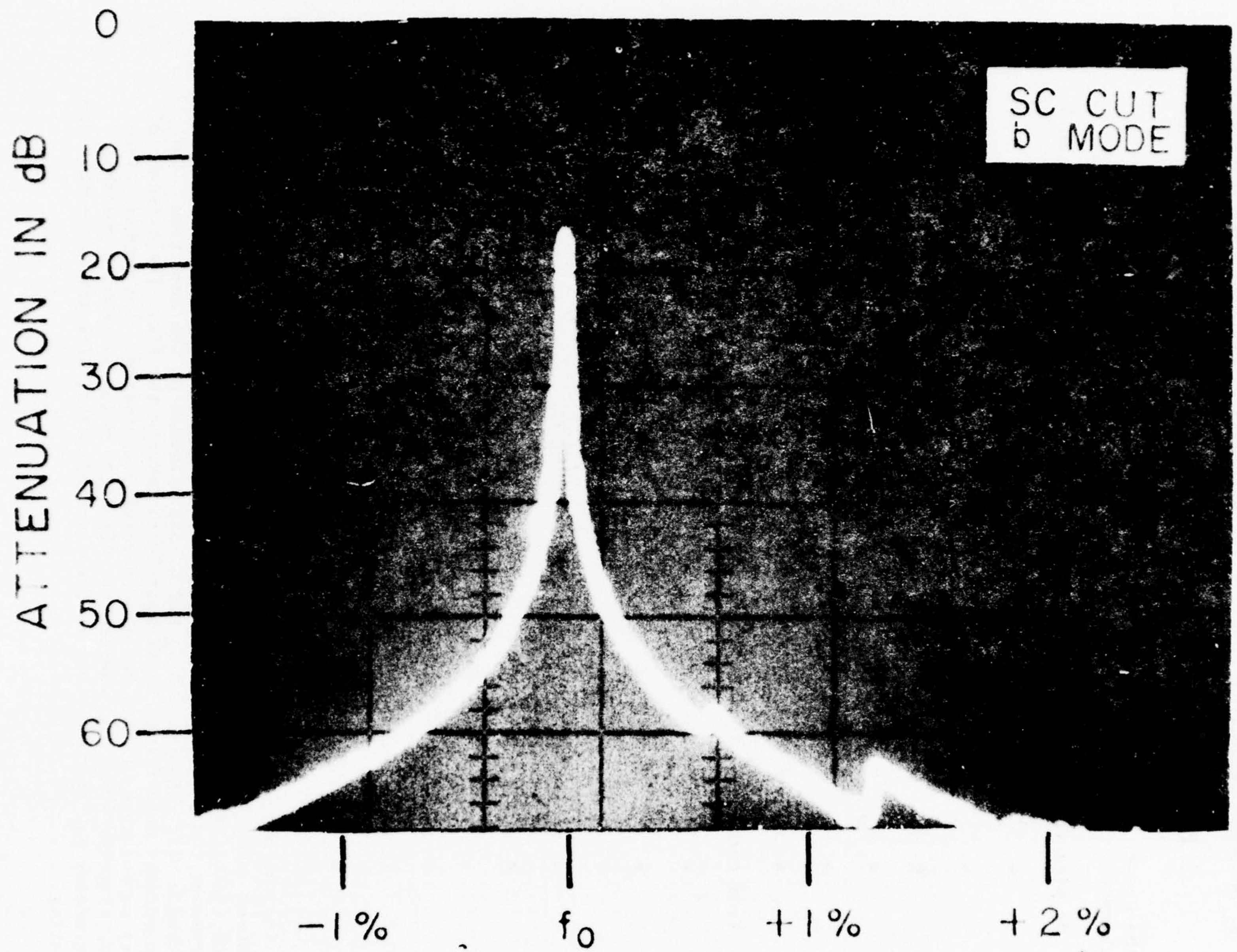


FIGURE 9. NARROWBAND MODE SPECTROGRAPH FOR THE SC-CUT B-MODE.

- Motional resistance constant (resistivity of motional resistance):

$$\rho_1 = R_1 A_e / t_a = 146 \;\; \Omega\text{-mm}.$$

In the above, $A_e = \pi\Phi_e^2/4$ is the electrode area, and $t_a$ is the plate thickness.

We pick for illustration the measured characteristics of resonator SC-4:

- $f_R^{(1)} = 5.937$ MHz
- $t_a^{-1} = 3.304$ mm$^{-1}$
- $\Phi_a = 14.18$ mm
- $C_o = 3.79$ pF
- $C_1 = 5.91$ fF
- $R_1 = 55 \;\; \Omega$.

From these measurements we deduce the following *effective* values:

- $\Phi_a/t_a = 46.9$
- $r^{(1)} = 641$
- $\tau_1 = 325$ fs
- $\Phi_e$ (effective) $= (4 t_a C_o/\pi\varepsilon)^{\frac{1}{2}} = 6.06$ mm
- $A_e/t_a = 95.3$ mm
- $\Gamma_1 = 62.0$ fF/m
- $\rho_1 = 5.24 \; \Omega$-m
- $Q = 1/\omega\tau_1 = 82{,}500$
- $\Psi = \Gamma_1$ (effective)$/\Gamma_1$ (theoretical) $= 77.3\%$.

In the above the effective electrode diameter $\Phi_e$ was determined from the measured value of $C_o$. The measurement of $C_o$ and $C_1$ was carried out on an RX Meter (schering bridge) using a frequency synthesizer. In the vicinity of resonance, the parallel capacitance versus frequency curve approximates a hyperbola very closely, and $C_o$ and $C_1$ are obtained at the same time. Our measurements were fit by least-squares to improve the fit. The presence of stray capacitance effects was also carefully minimized. The nominal electrode diameter was 5 mm, whereas the effective value is about 6 mm; the discrepancy may be partly due to the electrode tabs, with some component due to stray.

It is interesting to compute the values of $C_1$, $R_1$, and Q that would result in the ideal case of uniform distribution of motion and all losses due solely to bulk wave attenuation due to the viscosity. The results are:

- $C_1 = C_o/r^{(1)}$ (theoretical) = 7.64 fF
- $R_1 = \rho_1$ (theoretical) $\cdot\ t_a/A_e$ = 1.53 Ω
- $Q = 1/\omega_R\ \tau_1$ (theoretical) = 2.29 X10$^6$.

Taking into account the nonuniform distribution of motion with Ψ, the motional resistance would become (again assuming all loss is due to viscosity):

- $R_1 = R_1$ (theoretical)/Ψ = 1.98 Ω.

Most of the loss in this resonator is due to factors other than the bulk wave viscosity. In fact, since

- $\tau_1$ (effective)/$\tau_1$ (theoretical) = 27.8,

the bulk wave component is only (1/26.8) or less than 4% of the total.

At present, the apportionment of the losses in doubly rotated resonators is largely an open question. It was observed, however, that those SC-cut resonators having the electrode tabs running along Z" had resistance values from three to ten times smaller than those with tabs aligned along X". This points to energy being carried away to the mounting at the plate edges. Associated with this is the fact that the doubly rotated cuts in quartz do not support pure modes, such as the AT-cut mode. This means that the SC-cut c-mode consists in particle motion that is out of the plane of the plate. Considering the plate axes as the reference set, and performing $\phi$ and $\theta$ rotations with respect to this plate reference coordinate system, the angles $\phi_d$ and $\theta_d$ of the particle displacement for the SC-cut c-mode are:

- $\phi_d$ = 8.57°
- $\theta_d$ = 13.7°

The out-of-plane displacements are not negligible and certainly represent, for plano-plano resonators as described here, a significant mechanism for energy loss to the ambient fluid and the mounting system. Beveling or contouring the resonators and operation in a vacuum enclosure would decrease the size of these losses.

Energy trapping is another useful tool for keeping the Q high, as well as maintaining a clean mode spectrum; the energy-trapping rules for doubly rotated plates have yet to be worked out.

Additional work must also be done to calculate the frequency-wavelength dispersion diagrams for doubly rotated resonators. If the ratio $\Phi_a/t_a$ used happens to fall at a position where there is, e.g., strong coupling to flexure waves propagating laterally across the plate, then energy would be carried from the desired mode into the unwanted motion.

## MATHEMATICAL MODELING

An overview of the present theoretical work, compared to past treatments, is shown in Figure 10.

Past theoretical analyses[3,5,19,21] of static mechanical stress bias effects, in general, and of force sensitivities, in particular, have been two-step calculations. First, linear elastic solutions for the distribution of static mechanical stress bias in the resonator blank were obtained assuming that α-quartz is isotropic. These isotropic static solutions for the stress at the blank center were then used to calculate resonant frequency shifts in nonlinear wave propagation calculations which included the correct anisotropy of quartz and third-order elastic constant effects.

The present work is a two-step calculation where an attempt is made for a better solution to the static problem. The calculus of variations (essentially the Rayleigh-Ritz method)[50*] is used to find approximate solutions to the anisotropic static stress problem. The approximate static solution for the stress at the blank center is used in a nonlinear elastic wave propagation code to calculate resonant frequency shifts.

The present theoretical results for the singly-rotated AT- and BT-cuts provide a much improved comparison with published experimental results than the earlier theoretical results. The theory is used to calculate force sensitivity coefficients for the doubly rotated family containing the important AT- , FC- , IT- , and SC-cuts. The results provide the crystal designer with the appropriate azimuthal angle to mount the resonator on a two-point mount for minimum force sensitivity.

### A. Theory

One calculational approach that has been useful on numerous occasions for calculating stress patterns in static and vibrating elastic material bodies is the calculus of variations.[51,52*] The method is approximate, although the closeness to which the approximate solution can be brought to the actual solution is a matter of degree depending on the choice of trial (basis) functions, available computer size, and patience. The method for static problems amounts to formulating the total elastic stress-strain energy stored in a given body for the given boundary conditions and trial functions and then adjusting the trial functions to minimize the stored elastic energy. The approximations obtained with the method are somewhat better for the elastic energy values than for the stress distributions, but sufficient accuracy of the stress distributions can be obtained for practical considerations.

The total stored elastic energy L is given by

$$L = \frac{1}{2}\iiint_V dV\, S_\mu S_\lambda C_{\mu\lambda} - \iint_S dS\, F_i U_i \tag{1}$$

Here V and S are the resonator blank volume and surface, $C_{\mu\lambda}$ is the elastic stiffness tensor in engineering notation, $F_i$ is the distribution of force per unit area acting on the surface, $U_i$ is the elastic displacement vector. We use a cartesian coordinate system $x_i$ for the plate, and

*See list of references on p. 42.

## MATHEMATICAL MODELING OF FORCE-FREQUENCY EFFECT

<u>PRIOR</u>

- ISOTROPIC INITIAL STRESS FIELD ASSUMED.
- ANALYSIS LIMITED TO ROTATED-Y-CUTS $(YX\ell)\theta$.

<u>PRESENT</u>

- ANISOTROPIC INITIAL STRESS FIELD OBTAINED BY CALCULUS OF VARIATIONS.
- SOLUTION APPLIED TO DOUBLY ROTATED CUTS $(YXw\ell)\Phi/\theta$.

FIGURE 10. SYNOPSIS OF FORCE-FREQUENCY EFFECT MODELING.

$$S_{ij} = (U_{i,j} + U_{j,i})/2. \tag{2}$$

Here $\lambda$ and $\mu$ run 1-6, and i and j run 1-3. $S_\mu$ is related to $S_{ij}$ by the conventional[51] relations between engineering and tensor notations.

The present calculations treat a circular resonator blank of diameter d and thickness $\tau$ described by the IRE standard[46] notation $(YXw\ell)\phi/\theta$. We consider only contoured or energy-trapped resonator designs where the vibrational acoustic energy is restricted to the vicinity of the blank center. Contouring effects are ignored for the static stress distribution calculation, however, so that the much simpler problem of a flat circular plate can be solved for the static stress distribution. This simplification is warranted because the thin resonator blanks used for thickness shear resonators allow the assumption that the thickness dimension is small enough for a plane stress problem.

In the case of plane stress, $\lambda$ and $\mu$ run 1, 3, 5 and i and j run 1, 3, in Equations 1 and 2 ($x_2$ is blank thickness direction, $x_1$ is $\ell$, $x_3$ is w in the standard notation). Also, $C_{\lambda\mu}$ is replaced by $\gamma_{\lambda\mu}$, the planar elastic stiffness coefficients expressed in the plate coordinate system. Hence:

$$L = \frac{\tau}{2}\iint dx_1 dx_3 dV\ S_\mu S_\lambda \gamma_{\mu\lambda} - \iint_S dS\ F_i U_i \tag{3}$$

The variational method involves substituting a linear superposition of trial functions for $U_i$ into Equations 2 and 3, carrying out the integrals in Equation 3, and minimizing the resulting expression (differentiating the expression with respect to a given coefficient and setting that equal to zero) with respect to the coefficients of the trial functions. The problem then becomes a linear algebra problem in the coefficients. The choice of trial functions must be such that they represent a pointwise complete set over V and S. If the trial functions already satisfy some aspect of the problem such as the differential equation or boundary conditions, the number of trial functions needed for adequate convergence is small. For the present case, we take the easy way out and choose a simple power series expansion for $U_i$ and rely on the computer to handle large numbers of trial functions. The trial functions chosen for the two-point problem are

$$U_1 = \sum_{m,n,p,q=0}^{MNPQ} \left\{ A_{mn}\, x_1^{2m+1}\, x_3^{2n} + B_{pq}\, x_1^{2p}\, x_3^{2q+1} \right\}, \tag{4}$$

and

$$U_3 = \sum_{pqtu}^{PQTU} \left\{ B_{pq}\, x_1^{2p+1}\, x_3^{2q} + D_{tu}\, x_1^{2t}\, x_3^{2u+1} \right\} . \tag{5}$$

The value for $F_i$ is set equal to

$$F_i = F/(\delta\tau), \tag{6}$$

where F is the inwardly acting force applied to the opposite ends of a blank diameter, $\tau = t_a$ is the plate thickness, and $\delta$ is some length dimension which is small relative to the blank circumference (point force). All the integrals can be carried out in Equation 3, the surface integral being treated in the limit of a point force ($\delta \rightarrow 0$). After differentiation with respect to $A_{mn}$, $B_{pq}$, and $D_{tu}$, the resulting linear algebra problem has a solution for $A_{mn}$, $B_{pq}$, and $D_{tu}$, which scales with F. Thus, the static stress distribution can be solved for any known $\gamma_{\mu\lambda}$. A computer code for the linear algebra problem was written which included rotation of the quartz elastic tensor to obtain $\gamma_{\lambda\mu}$ and arbitrary selection of M, N, P, Q, T, and U. From symmetry arguments, one is led to use groups of the trial functions, adding new groups until satisfactory convergence is obtained. The groups are defined by (O,R), where the group includes all pairs of (m,n), (p,q), and (t,u) with the first member increasing from zero to R in steps of one while the second member decreases from R towards zero in steps of one; e.g., (0,3), (1,2), (2,1), (3,0) make up the family (0,3).

The resulting solution for the static stress at the plate center using the published $c^E_{ijkl}$ constants for quartz[53*] is incorporated into a previously described computer code[3,5] which calculates the resonant frequency shift caused by elastic nonlinearities (third-order elastic constant effects).[54*] We use here the definition for the force sensitivity coefficient $K_f$ defined as[20]

$$\frac{\Delta f}{f} = K_f \frac{FN_o}{d\tau} \tag{7}$$

where $N_o$ is the frequency constant. The plate diameter is $d = \Phi_a$. Units are $K_f$ in m·sec/N, $N_o$ in m/sec, d and $\tau$ in m, and f in $\sec^{-1}$ or Hz. $K_f$ is positive if frequency increases upon application of a compressive force.

The direction of the applied forces F is important because of the anisotropy of the quartz nonlinear elastic problem and because of the quartz anisotropy in the static stress problem (the latter is ignored in earlier isotropic static solutions). We choose to follow the earlier experimental work by presenting results for the $K_f$ of a given $(YXw\ell)\phi/\theta$ cut as a function of azimuthal angle $\psi$. The azimuthal angle is measured in right-hand convention about $x_2''$ from $x_1''$ (or $\ell$) in the plane of the plate: positive angle going from $x_1''$ to $-x_3''$, as seen in Figure 11. The direction of the applied force is therefore specified by $x_1''$ when it undergoes the rotations $(YXw\ell t)\phi/\theta/\psi$. The angles $\phi$, $\theta$, and $\psi$ are just the euler angles encountered in classical mechanics.[55*]

## B. Results

The program was first tested for isotropic blanks. The solution at the center of the plate converges rapidly (four significant figures) to that found analytically,[56*] i.e., $6F/\pi d\tau$ compression along the diameter aligned with (inwardly directed) F and $2F/\pi d\tau$ tension along the diameter perpendicular to F.

Calculations were carried out for the AT- and BT-cuts since there exist large amounts of force sensitivity data and considerable discrepancies between the data and earlier theoretical results for these cuts. The results

*See list of references on p. 43.

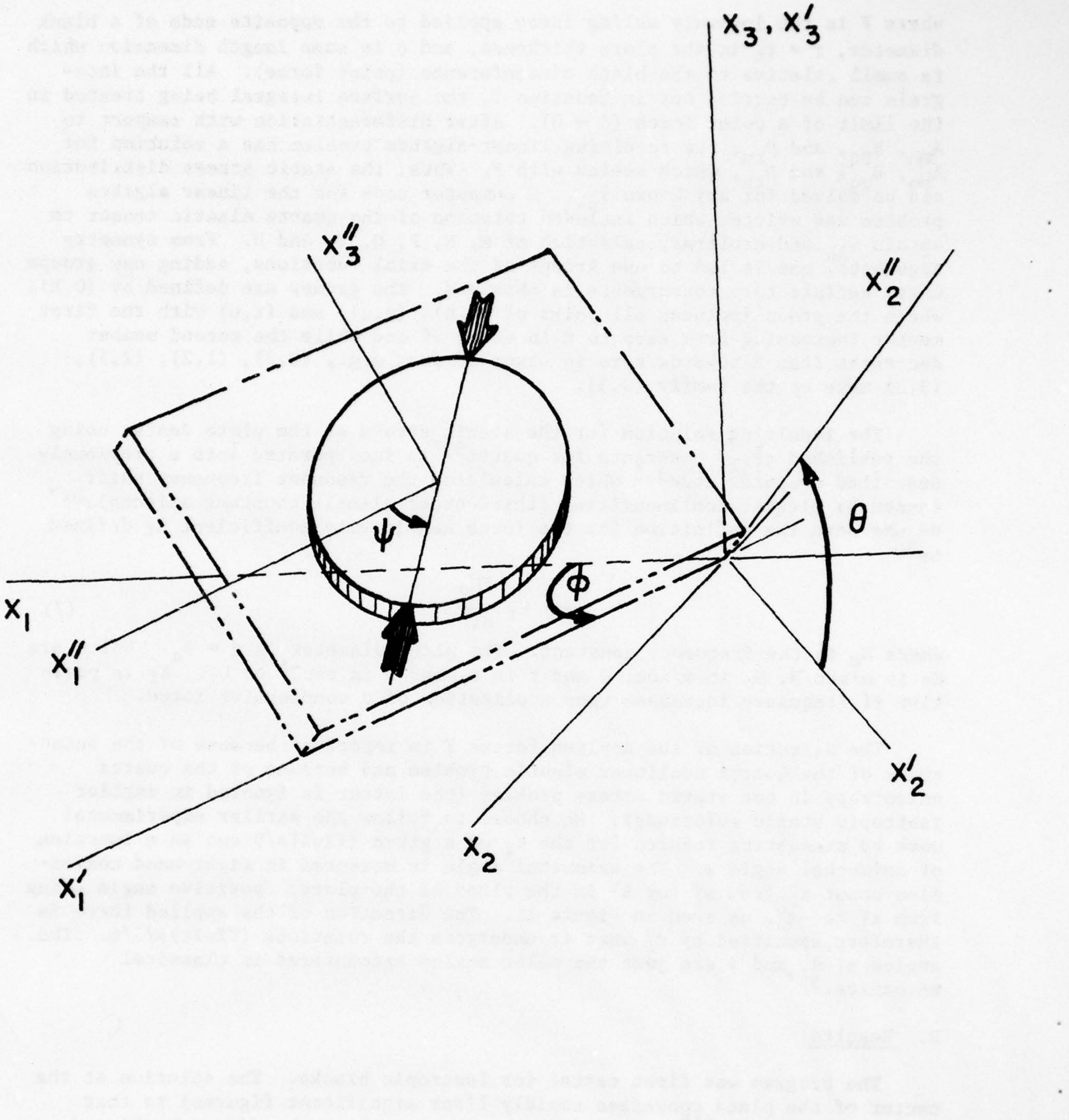


FIGURE 11. CONVENTION FOR SPECIFYING FORCE AXIS.

for the zero temperature coefficient thickness shear c-mode **are shown in** Figure 12 as $K_f$ vs. $\psi$. The "*isotropic assumption*" in Figure 12 is the result obtained in the present computer codes when the isotropic solution ($-6F/\pi d\tau$, $2F/\pi d\tau$) is used for the static stress pattern at the plate center. This result, which is representative of the best results obtained before the present work, is numerically equivalent to the results of Lee, et al.[21] Note the discrepancies between the isotropic assumption results and the experimental summary provided by Ratajski;[20] namely, the difference in value for $K_f$ at $\psi = 0$ for the AT-cut, and the complete failure to predict the dip in the BT-cut results. As seen in Figure 12, the present calculations using the variational treatment are quantitatively accurate at $\psi = 0$ for the AT-cut and predict a dip for the BT-cut. The calculations leading to Figure 12 involved using all the families up to and including (0,5), making 21 values each for $A_{mn}$, $B_{pq}$, and $D_{tu}$ for a 63 x 63 linear algebra problem. The addition of the (0,5) family only changed the numerical answer for the stress at the plate center in the third significant figure, so that some idea of convergence would be provided.

Figure 13 contains present results for the thickness-shear (mode c) IT-cut and previously published experimental results.[1] The qualitative features of the experimental data are reproduced by both the isotropic assumption results and the full variational result. In view of the results in Figure 12, where more experimental data exist, we consider the variational result to be the more accurate. The quantitative discrepancy between experiment and theory is not as serious as might appear in Figure 13 because there is a factor-of-two scale expansion between Figures 12 and 13 to account for the generally smaller $K_f$ values of doubly rotated cuts.

A series of calculations has been carried out for the zero temperature coefficient branch (mode c) subset within $(YXw\ell)\phi/\theta$: $\phi = 0°$ (AT-cut); $\phi = 10°$; $\phi = 15°$ (FC-cut); $\phi = 19.1°$ (IT-cut); $\phi = 21.9°$ (SC-cut); $\phi = 30°$ (rotated-X-cut). The results for $K_f$ vs. $\psi$ are shown in Figure 14. The curves drawn in Figure 14 are presented separately in Figures 15-20.

The family of curves for $K_f$ vs. $\psi$ in Figure 14 are the general theoretical results for this report. The curves should be useful in choosing the optimum location of bonding pads for two-point mounts to minimize the effects of mounting stresses and some effects of shock and vibration.

In Table 2 are given the computed angles $\psi$ at which $K_f$ is zero, as function of $\phi$. Table 3 lists the computed locations and values of the extrema of $K_f$ as function of $\phi$.

TABLE 2. ZEROS OF $K_f$

| $\phi°$ | $\psi°$ | $\phi°$ | $\psi°$ |
|---|---|---|---|
| 0 | 64.7 , 115.3 | 19.1 | 79.3 , 163.1 |
| 10 | 68.5 , 125.2 | 21.9 | 81.6 , 171.9 |
| 15 | 74.8 , 148.8 | 30 | 79.3 , 184.3 |

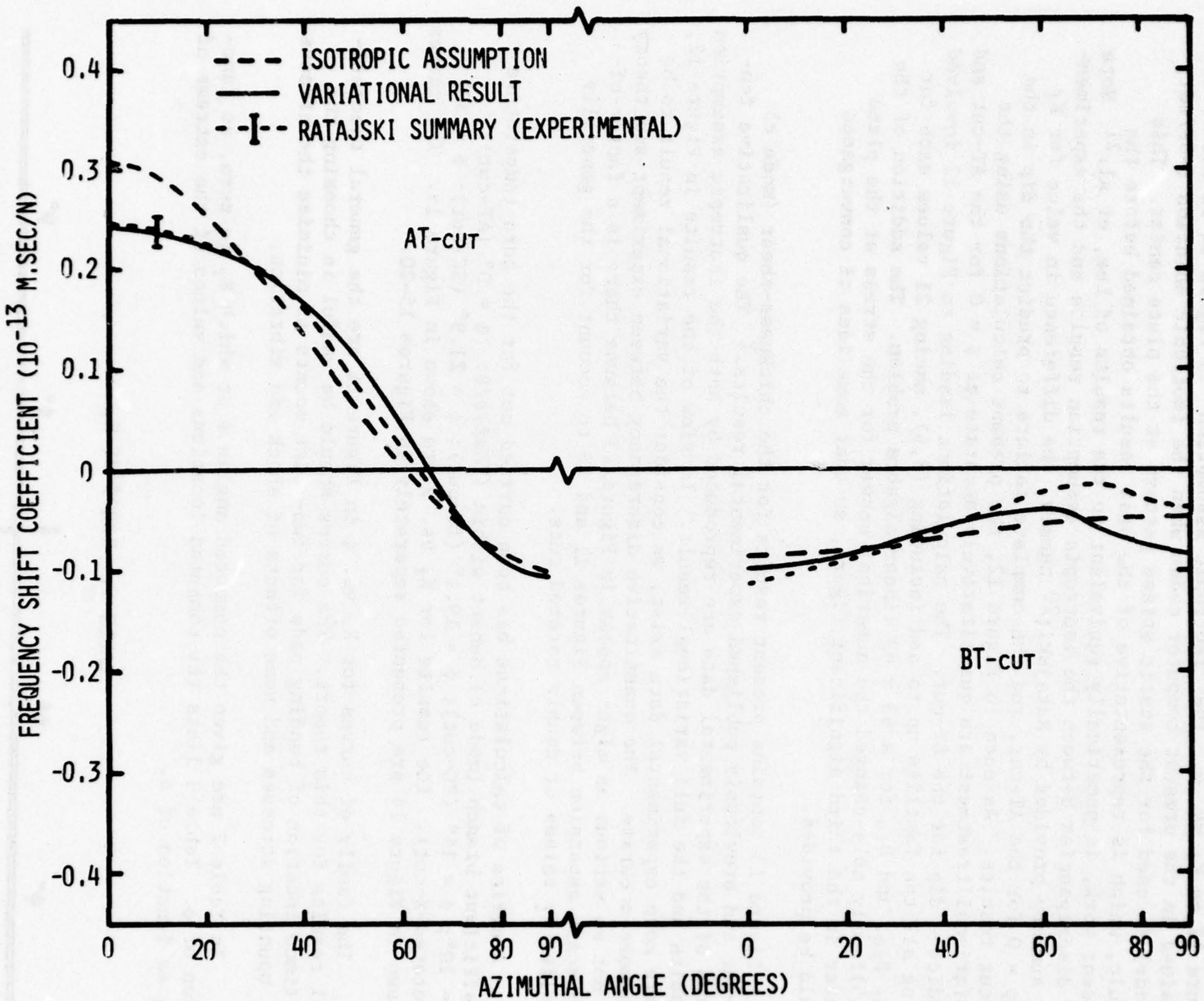


FIGURE 12. FORCE-FREQUENCY RESULTS FOR AT- AND BT-CUT QUARTZ.

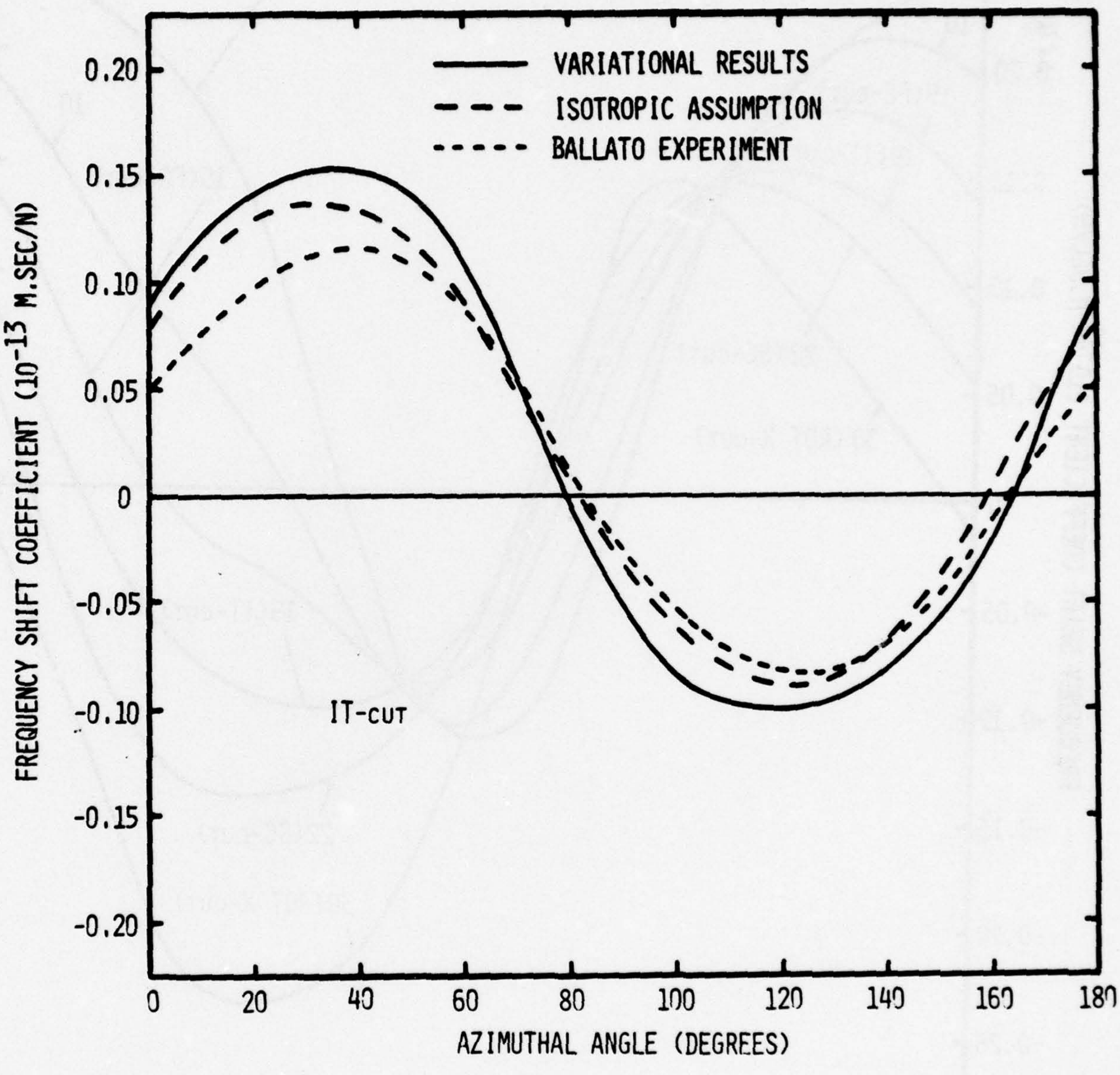


FIGURE 13. FORCE-FREQUENCY RESULTS FOR IT-CUT QUARTZ.

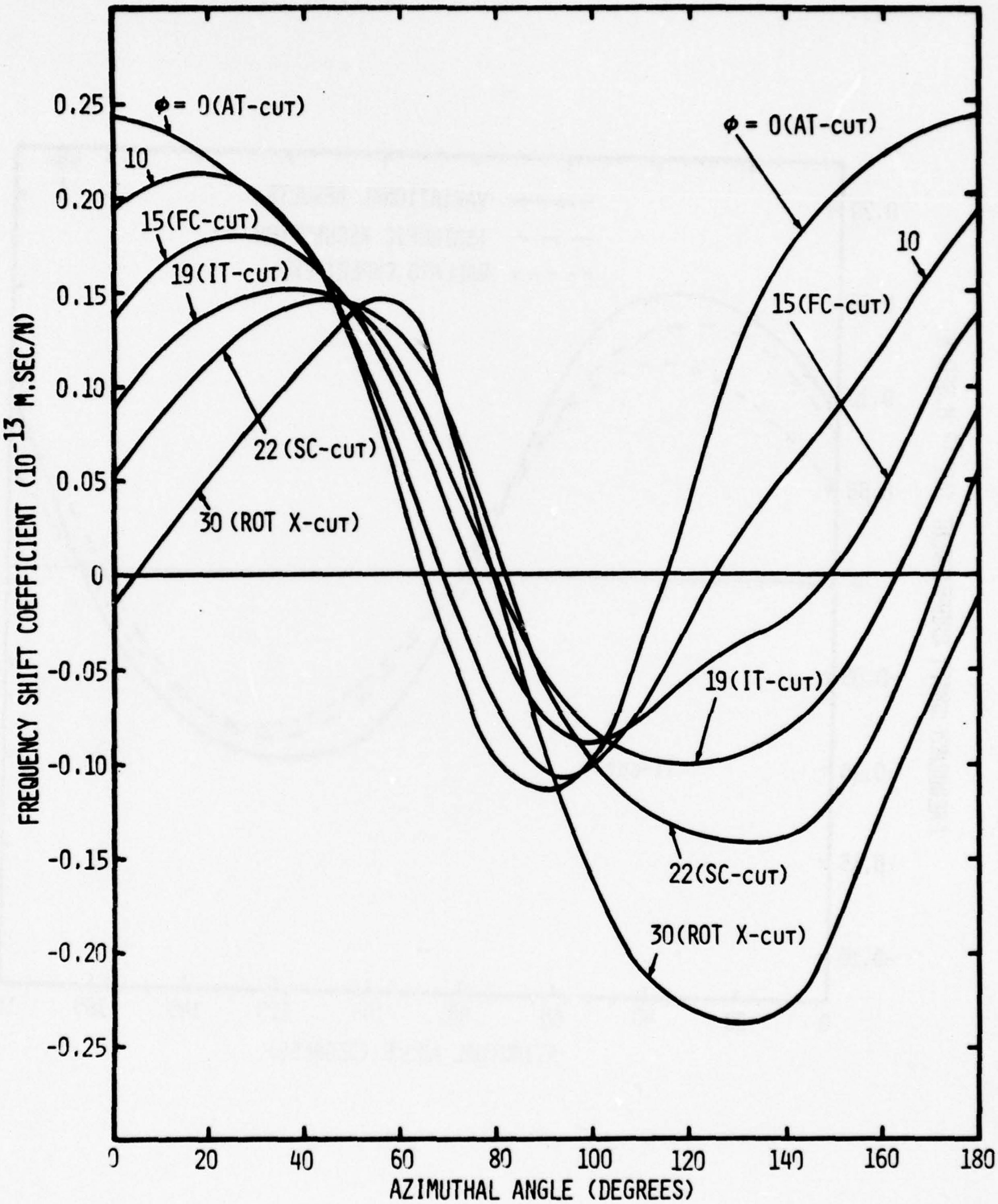


FIGURE 14. FORCE-FREQUENCY RESULTS FOR DOUBLY ROTATED QUARTZ CUTS.

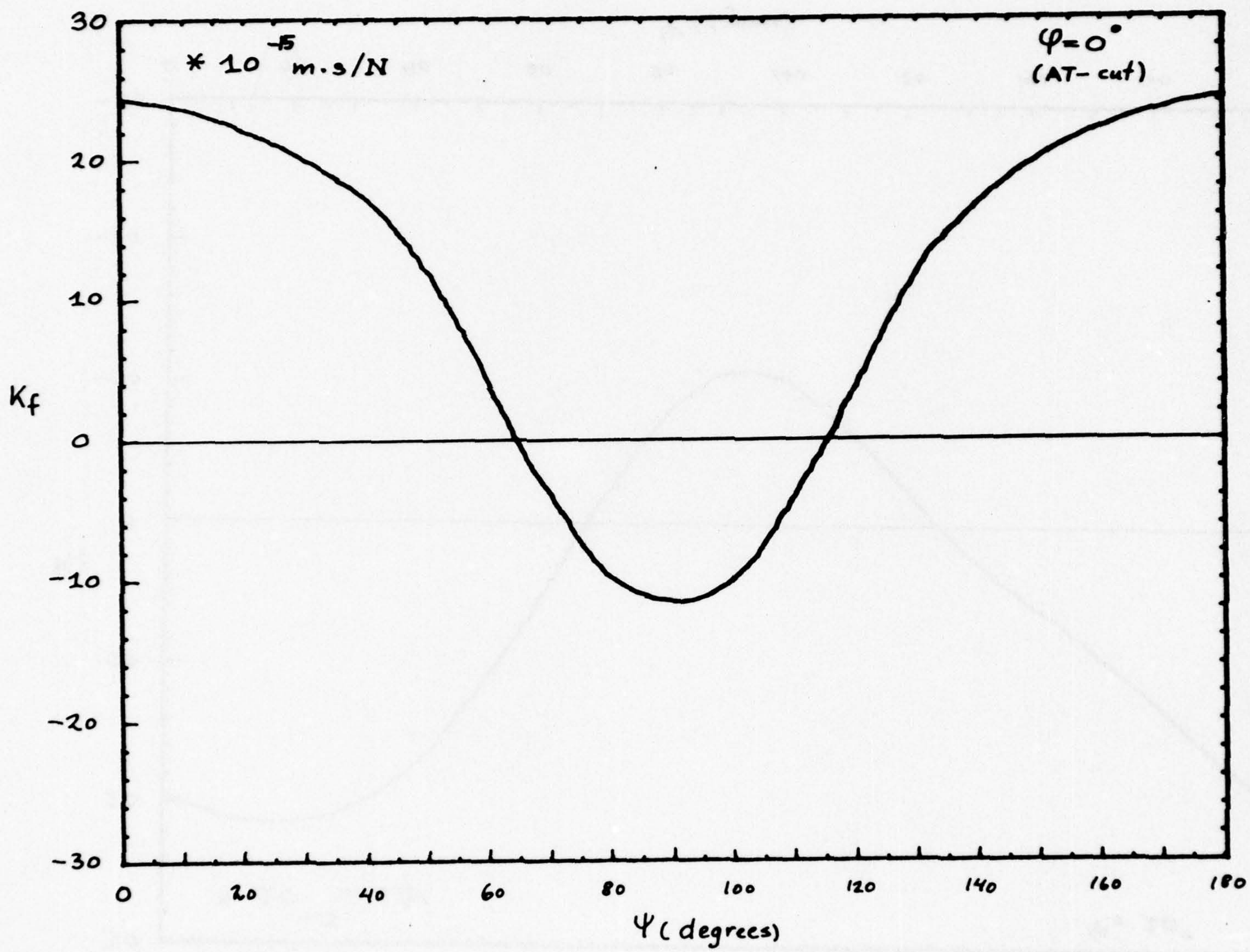


FIGURE 15. $K_F$ VERSUS PSI FOR PHI EQUALS 0 DEGREES.

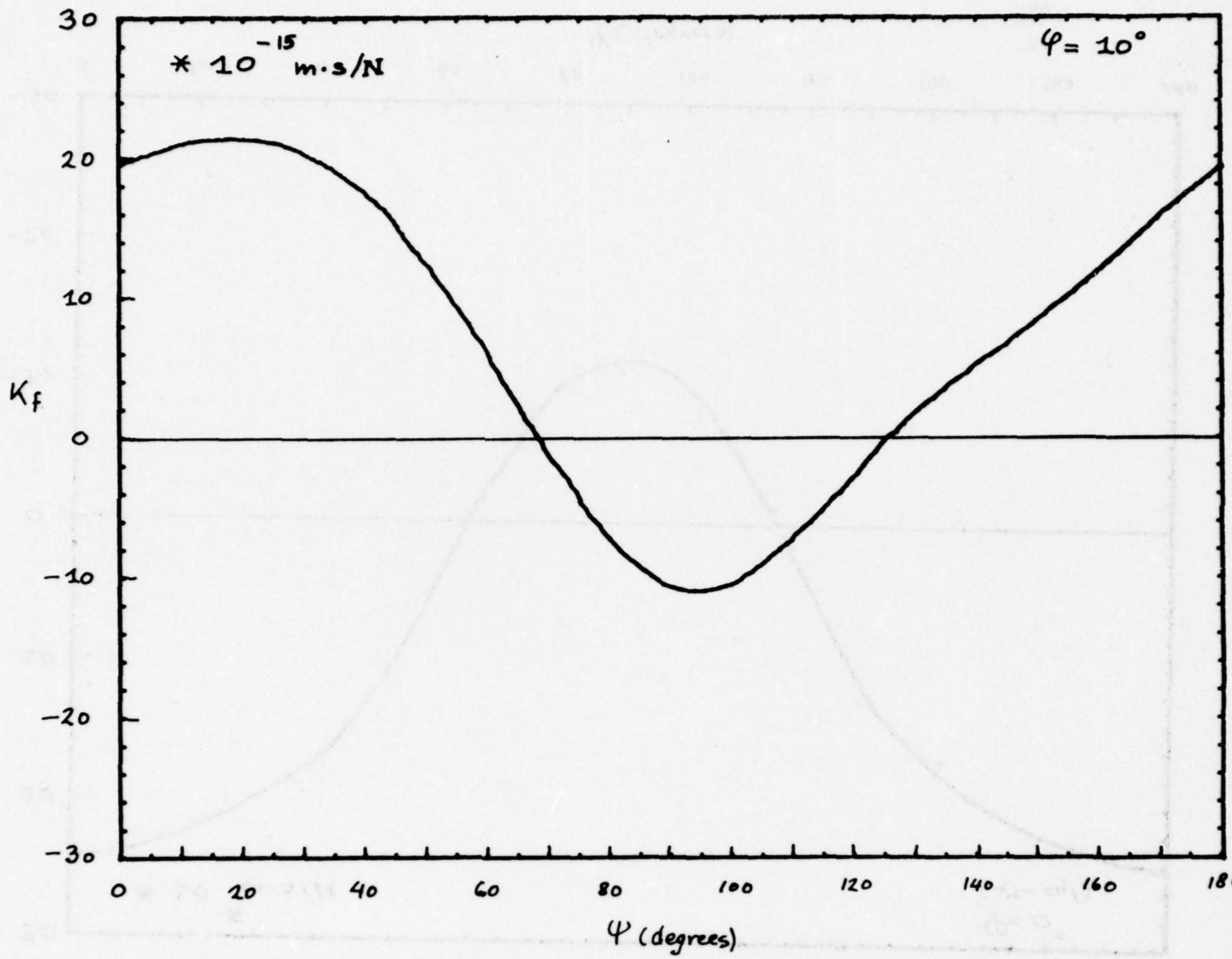


FIGURE 16. $K_F$ VERSUS PSI FOR PHI EQUALS 10 DEGREES.

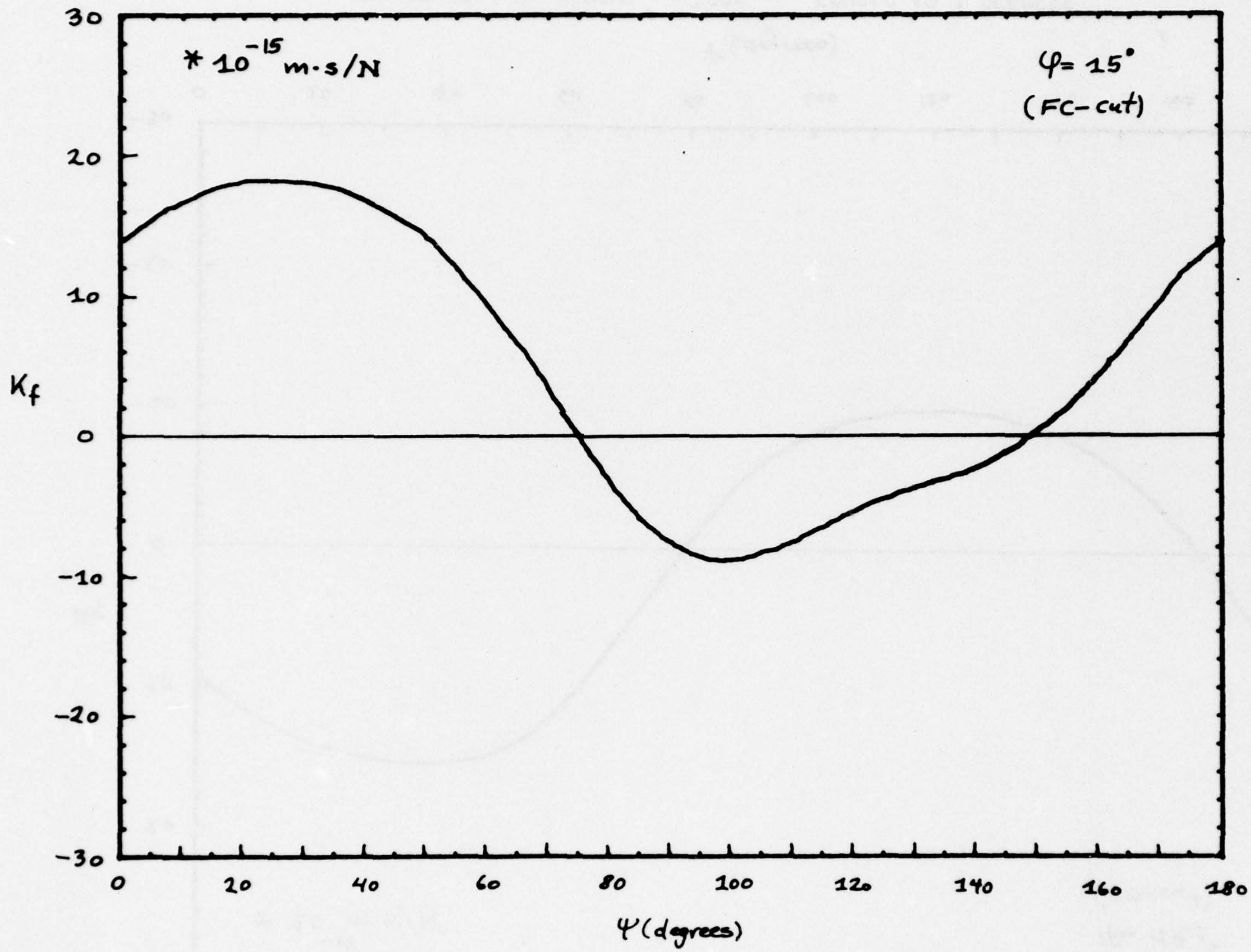


FIGURE 17. $K_F$ VERSUS PSI FOR PHI EQUALS 15 DEGREES.

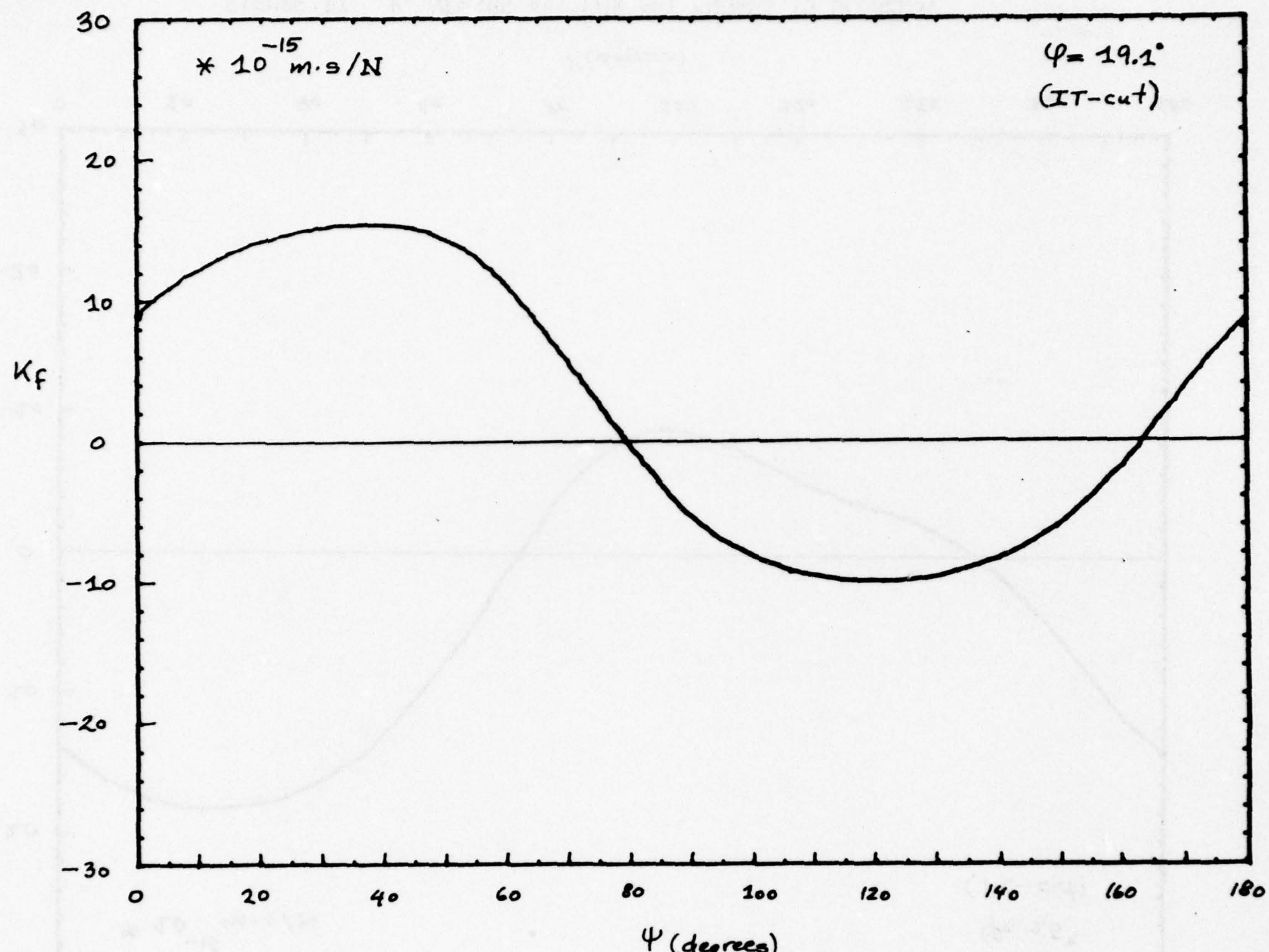


FIGURE 18. $K_F$ VERSUS PSI FOR PHI EQUALS 19.1 DEGREES.

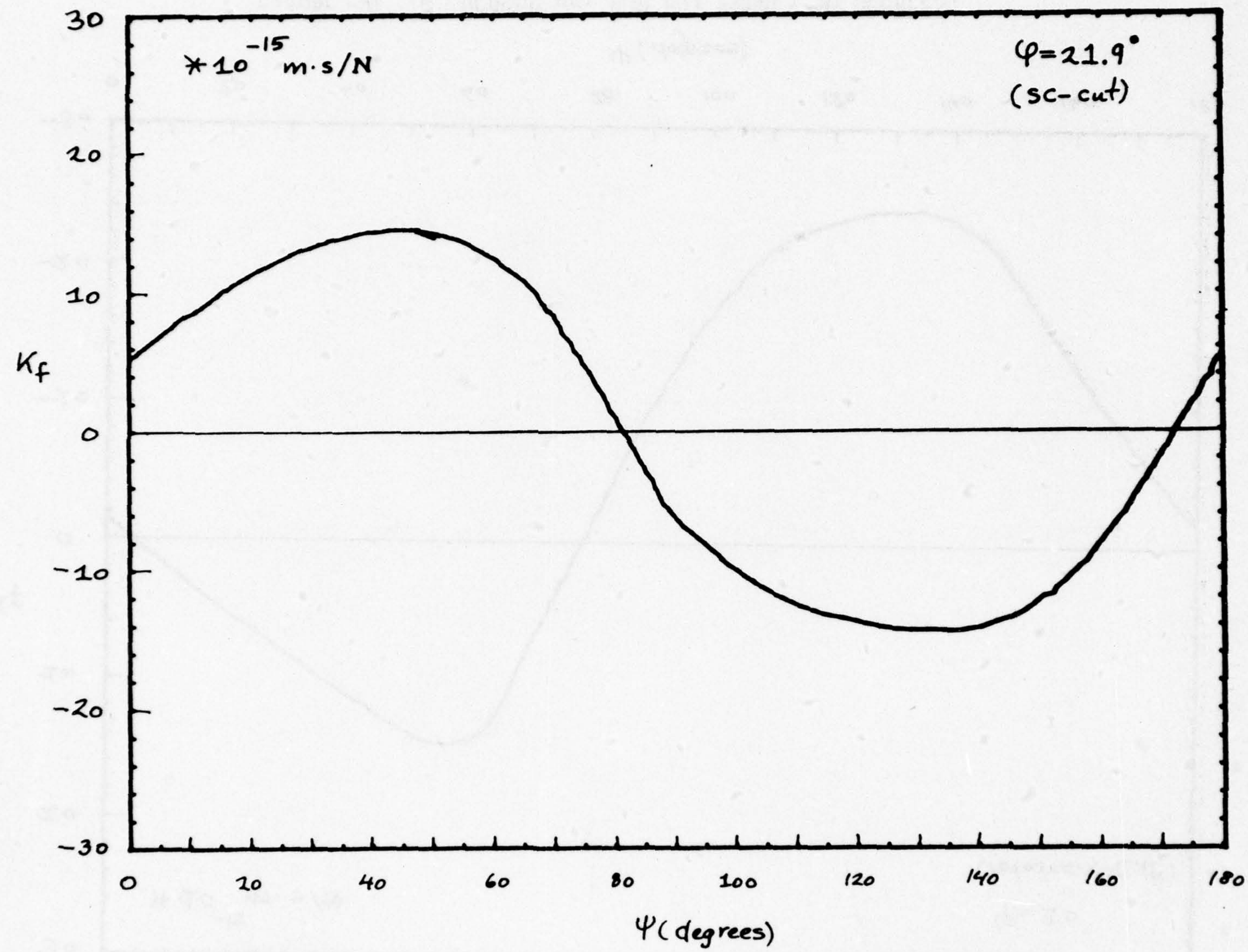


FIGURE 19. $K_F$ VERSUS PSI FOR PHI EQUALS 21.9 DEGREES.

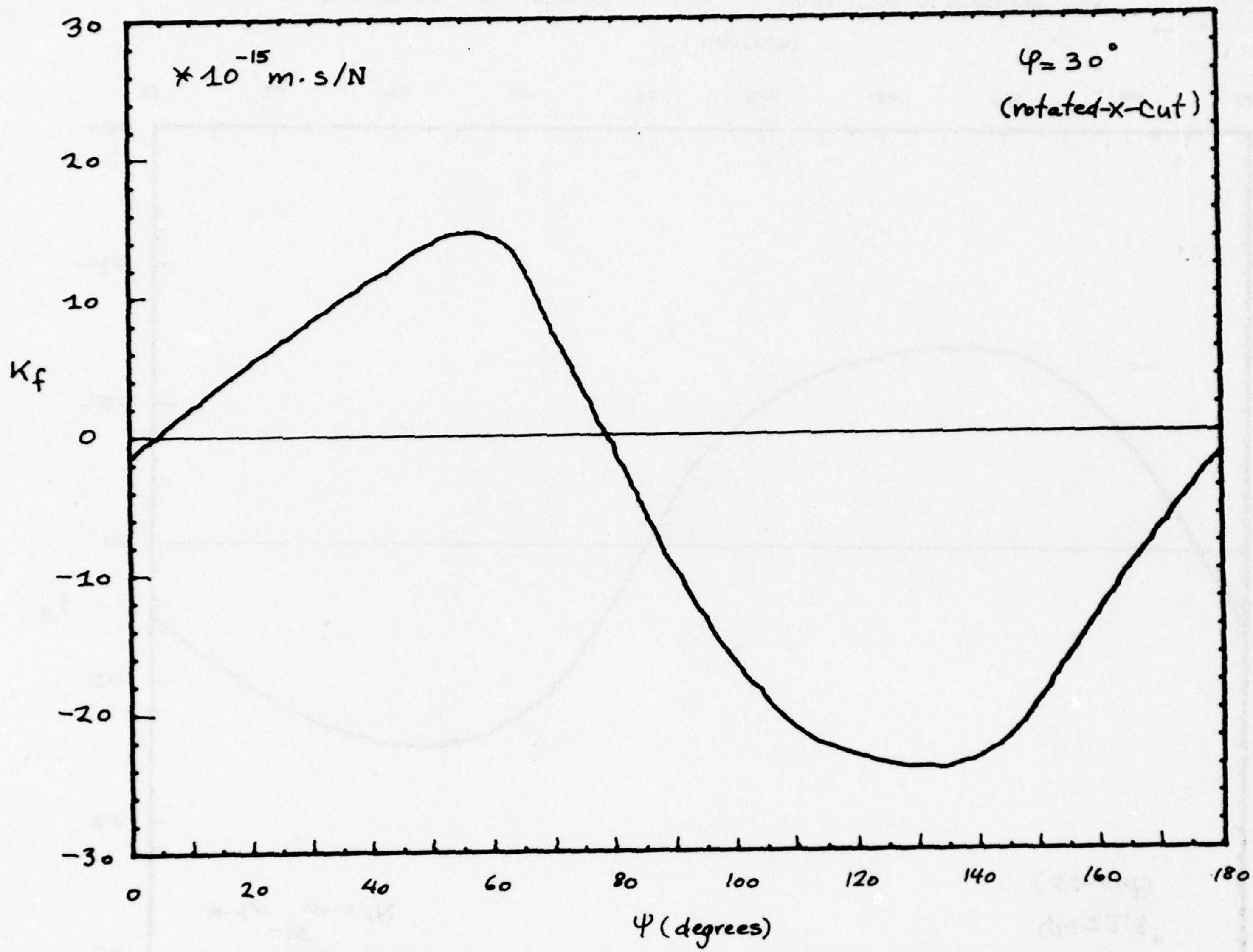


FIGURE 20. $K_F$ VERSUS PSI FOR PHI EQUALS 30 DEGREES.

TABLE 3. LOCATION AND VALUES OF $K_f$ EXTREMA

| $\phi°$ | $\psi°$ | $K_f$ (max) | $\psi°$ | $K_f$ (min) |
|---|---|---|---|---|
| 0 | 0 | 24.5 | 90 | -11.5 |
| 10 | 17.6 | 21.4 | 93.2 | -10.8 |
| 15 | 26.0 | 18.2 | 98.8 | - 8.9 |
| 19.1 | 36.6 | 15.3 | 118.1 | -10.1 |
| 21.9 | 44.3 | 14.7 | 131.6 | -14.3 |
| 30 | 55.6 | 14.7 | 130.0 | -23.9 |

($K_f$ in $10^{-15}$ m·s/N)

## EXPERIMENTAL CONFIRMATION

Apart from the IT-cut results obtained in 1960,[1] no experimental results were available for comparison with the theoretically predicted force-frequency curves of doubly rotated cuts of quartz, shown in Figure 14. In order to obtain these results, the experimental apparatus of Figure 21 was constructed. It contains provisions for the precise rotation of the angle $\psi$ by means of a vacuum chuck for holding the crystal (and maintaining strict crystal vertical alignment) and high-ratio reduction gear. Five mil wires are bonded to the crystal and serve for the electrical connections. To the left in the figure, the connections are brought out to a Crystal Impedance Meter (RFL model 459 = TS-330 with low drive modification[57*]). The frequency is recorded from a counter.

Micrometer adjustments are available for assuring accurate alignment of the various portions of the jig. Force application was made by a movable rod on which calibrated masses were applied; the mass of the rod was taken into account. The overall setup is shown in Figure 22.

The crystals considered here had orientations (YXwℓ)$\phi/\theta$, with $\phi$ = 10°, 15°, and 21.9°, and $\phi$ such that the units had zero temperature coefficients ($\phi \simeq +34°$). All crystal units were provisionally scored near the $X_3''$ axis (projection on the Z, or optic, axis). The true location of $X_3''$ with respect to the score mark was later determined for each crystal to within 1° by a conoscope, and enabled $\psi$ to be accurately known. (This procedure was also applied to the still-extant IT-cut crystal that was described in Reference 1. The new measurement disclosed that the true $X_3''$ axis as seen in the conoscope was a full 19° in error with respect to the score mark on the crystal. Thus, the curve in Figure 18 of Reference 1 ought to be translated to the right with respect to the graph axes, so that the zeros occur at 85° and 163°. This finding was a welcome resolution of a disturbing discrepancy between theory and experiment!)

Measurements were made in $\psi$ intervals of 10°. Three readings were taken at each $\psi$. First, the frequency of the unloaded vibrator was measured. Then the weight was lowered gently, and the loaded frequency was recorded. Finally, the frequency with the weight removed was measured. The first and third frequencies were, in all cases, at most one or two Hz apart. $K_f$ was

*See list of references on p. 43.

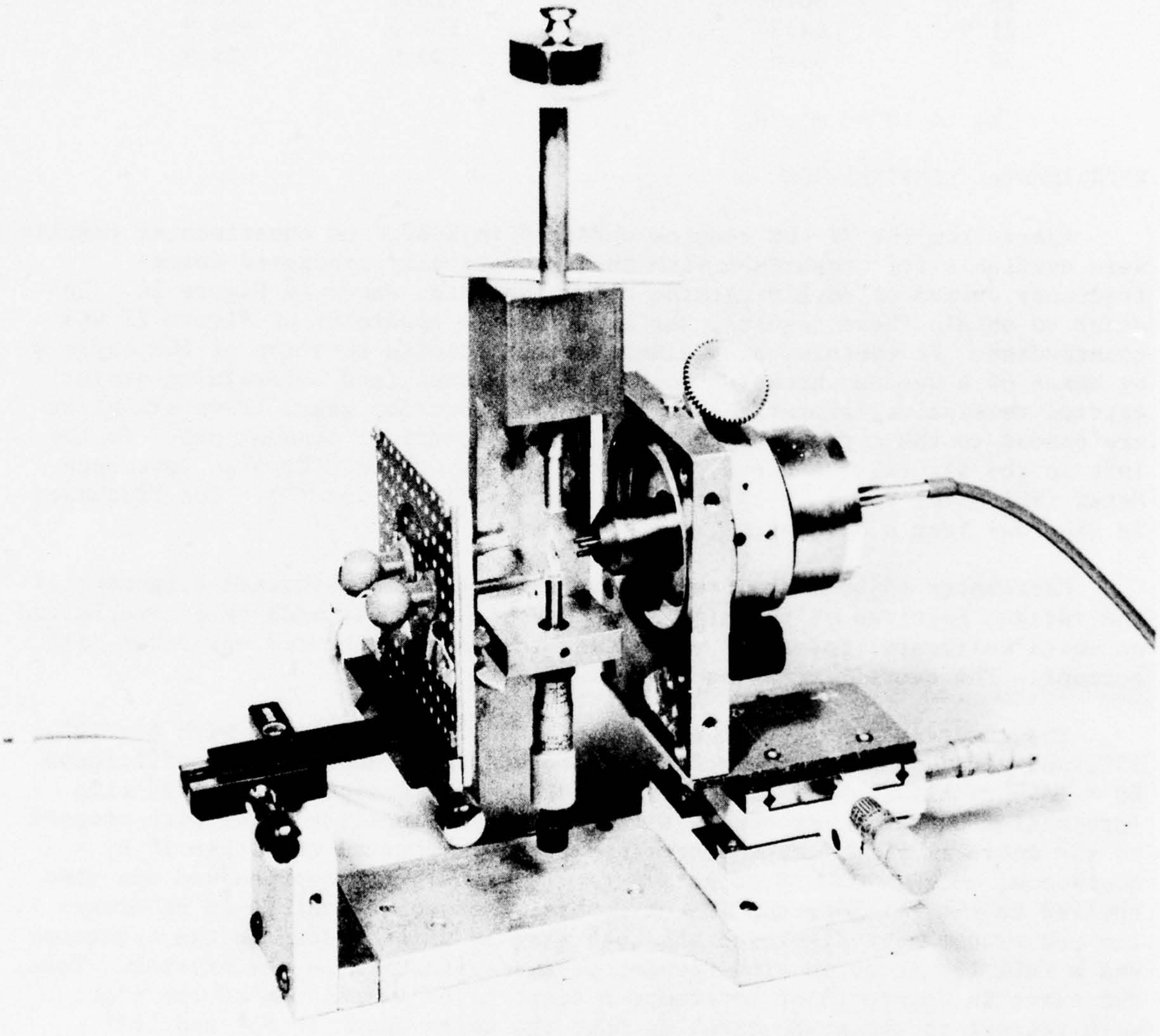

FIGURE 21. APPARATUS FOR APPLYING EDGE FORCE TO CRYSTAL.

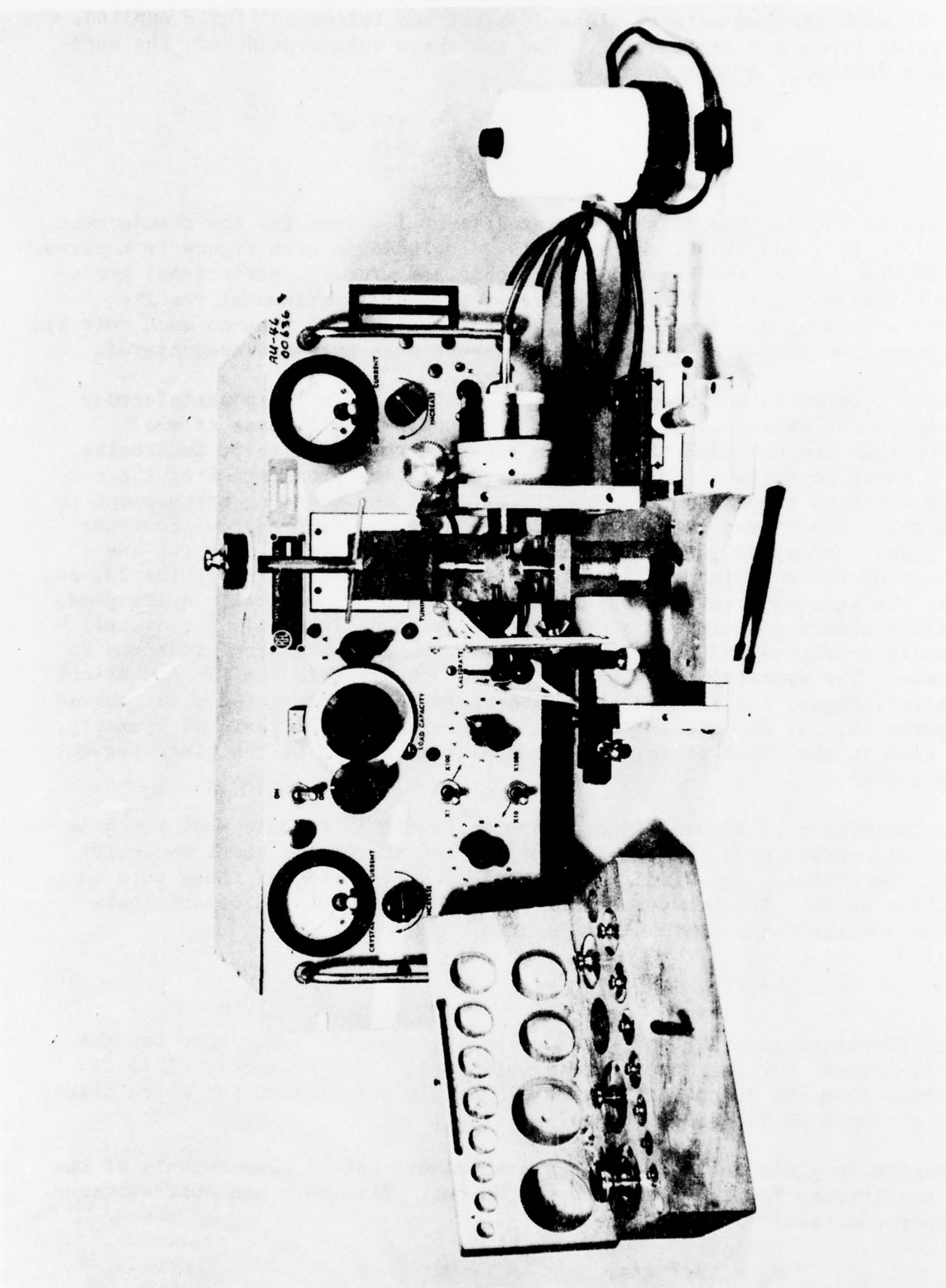

FIGURE 22. EXPERIMENTAL SETUP.

then calculated from equation (7) using the measured values of frequency change $\Delta f$ with applied weight, plate diameter and thickness, force applied, and crystal frequency constant $N_o$. For the three cuts considered, the antiresonance frequency constants are[13]

| | |
|---|---|
| $\phi$ = 10°, | $N_o$ = 1690 m/s |
| 15°, | 1726 |
| 21.9°, | 1797 |

Figures 23, 24, and 25 show the experimental curves for the c-mode cuts at $\Phi$ = 10°, 15°, and 21.9°, respectively. Included in each figure is a curve, shown dashed, of the theoretical result obtained from the variational procedure outlined earlier. The solid curves represent experimental results averaged over a group of units and also over a number of runs on each unit by three experimenters. The error bars represent data extremes encountered.

Data scatter is worst for the $\Phi$ = 10° units, and a fully satisfactory explanation for this cannot at present be given. In all cases it was observed that the unloaded frequencies appeared to vary with $\psi$, indicating, e.g., a stray capacitance effect due to the changing proximities of the connecting wires to the fixture. A modification of the mounting arrangement to reduce this effect produced the solid curve shown in Figure 25 without the error bars. As may be seen in the figure, the modification improves the agreement of the experimental curve with the theoretical. In Figures 23, 24, and 25, the agreement between experiment and theory is generally quite good, especially when the smallness of the effect is borne in mind. The overall magnitudes predicted and observed agree well, as do the general features in each case. The symmetry about $\psi$ = 0° and 90° observed in the AT- and BT-cut curves (cf. Figure 12) is seen to be absent in the doubly rotated cut curves of Figures 13, 23, 24, and 25; this is because the digonal axis of symmetry, which lies in the plane of rotated-Y-cut plates, is out of the plane for cuts having $\Phi \neq 0°$.

A comparison of Figures 24 and 25 with Figure 12 reveals that the peak-to-peak excursions of $K_f$ with $\psi$ for the FC- and SC-cuts is about one half that of the AT-cut. This indicates a reduced sensitivity of these cuts to mechanical shock. Further comparison between Figures 24 and 25 discloses that the average force coefficient

$$\langle K_f \rangle = \frac{1}{\pi}\int_0^{\pi} K_f(\psi)\, d\psi \tag{8}$$

for the FC-cut is positive and relatively large (albeit lower than for the AT-cut); whereas for the SC-cut it is very small (ideally zero). This feature stems from the SC-cut definition as the ZTC orientation for which planar stress produces no frequency change.

Figure 26 gives the results of a preliminary set of measurements of the force sensitivity for the b-mode of the SC-cut. This mode has antiresonance frequency constant[13]

$$N_o = 1977 \text{ m/s},$$

and a temperature coefficient of approximately -25 or -26 ppm/K. Because of

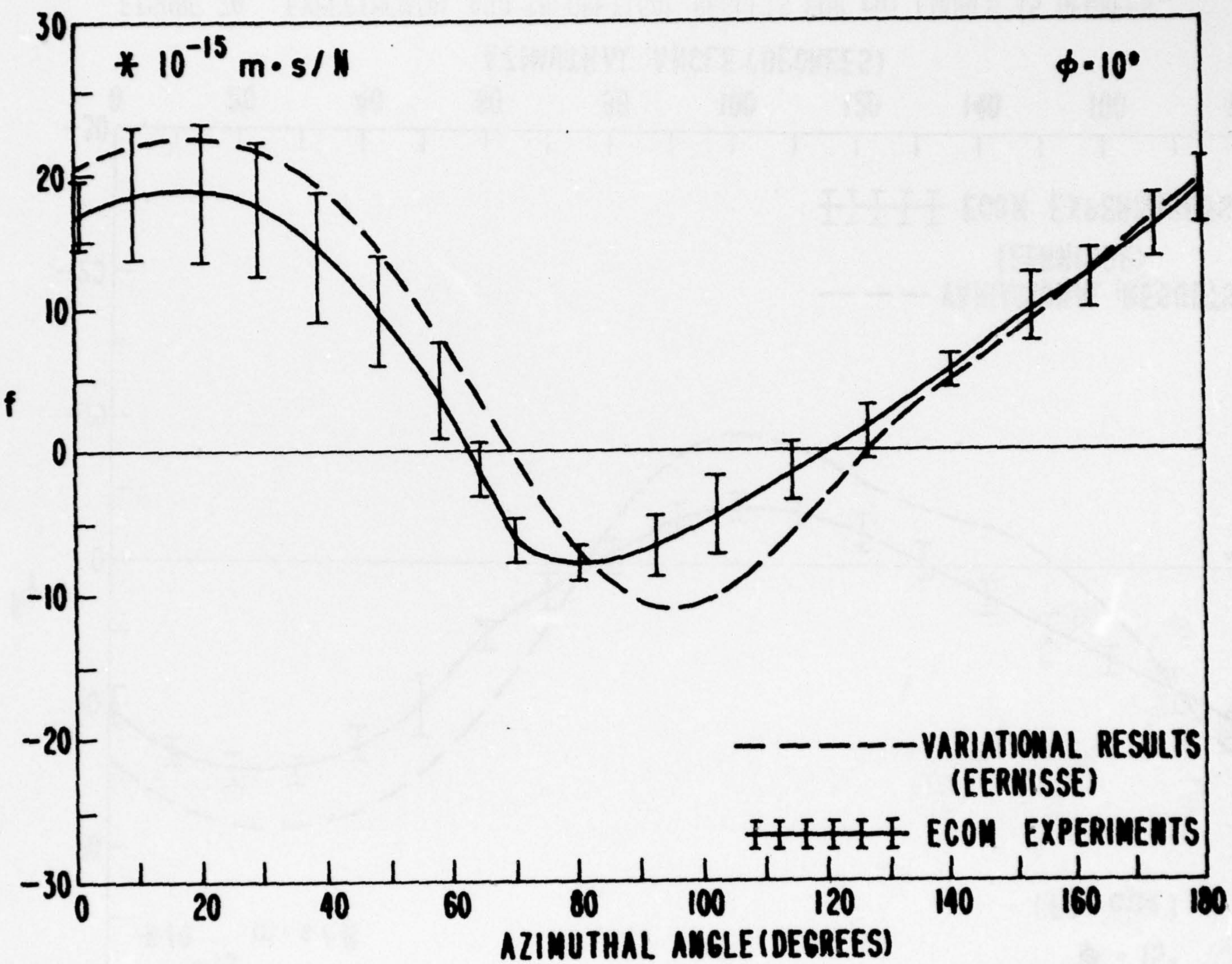


FIGURE 23. EXPERIMENTAL AND THEORETICAL RESULTS FOR PHI EQUALS 10 DEGREES.

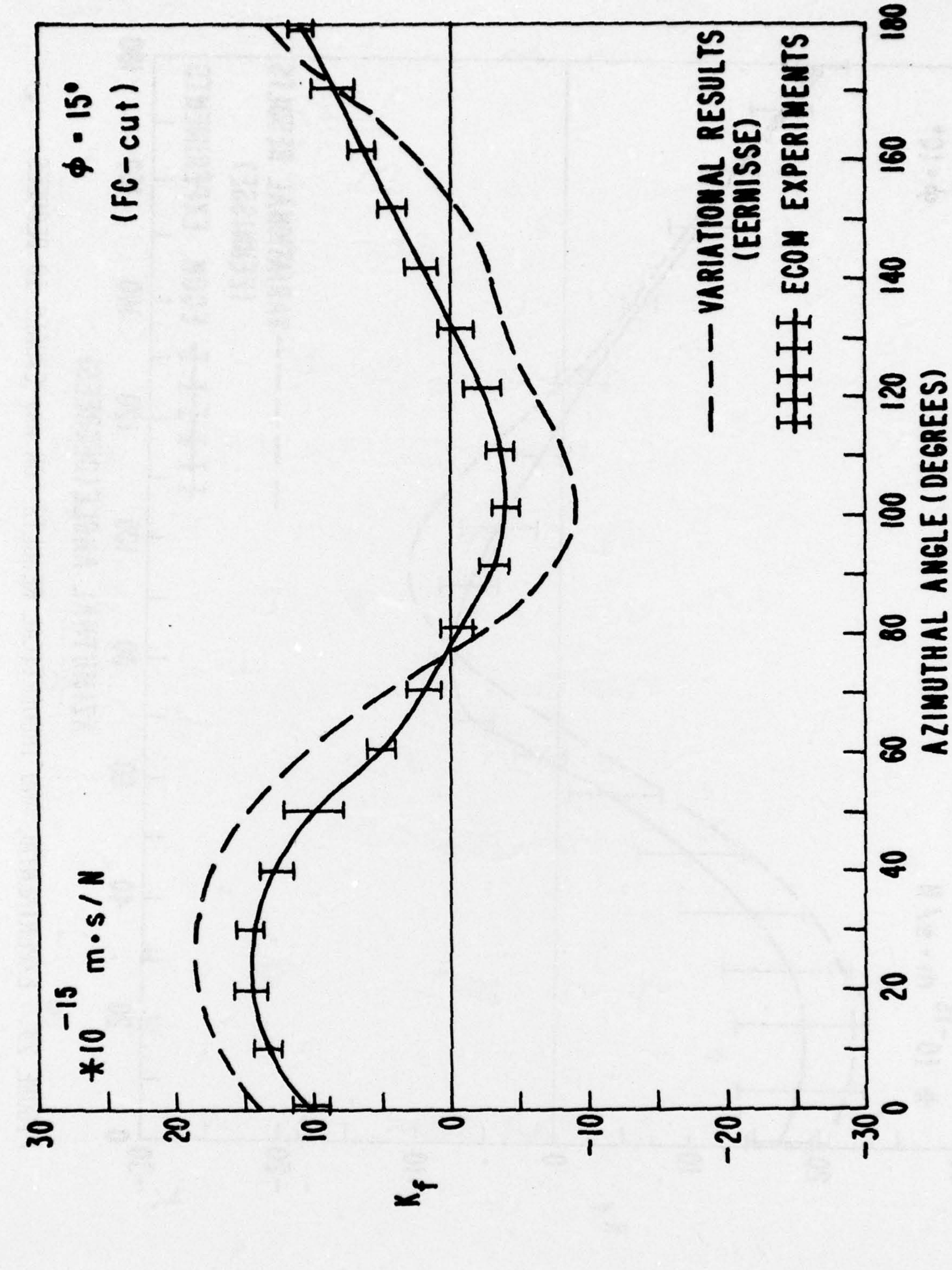


FIGURE 24. EXPERIMENTAL AND THEORETICAL RESULTS FOR PHI EQUALS 15 DEGREES.

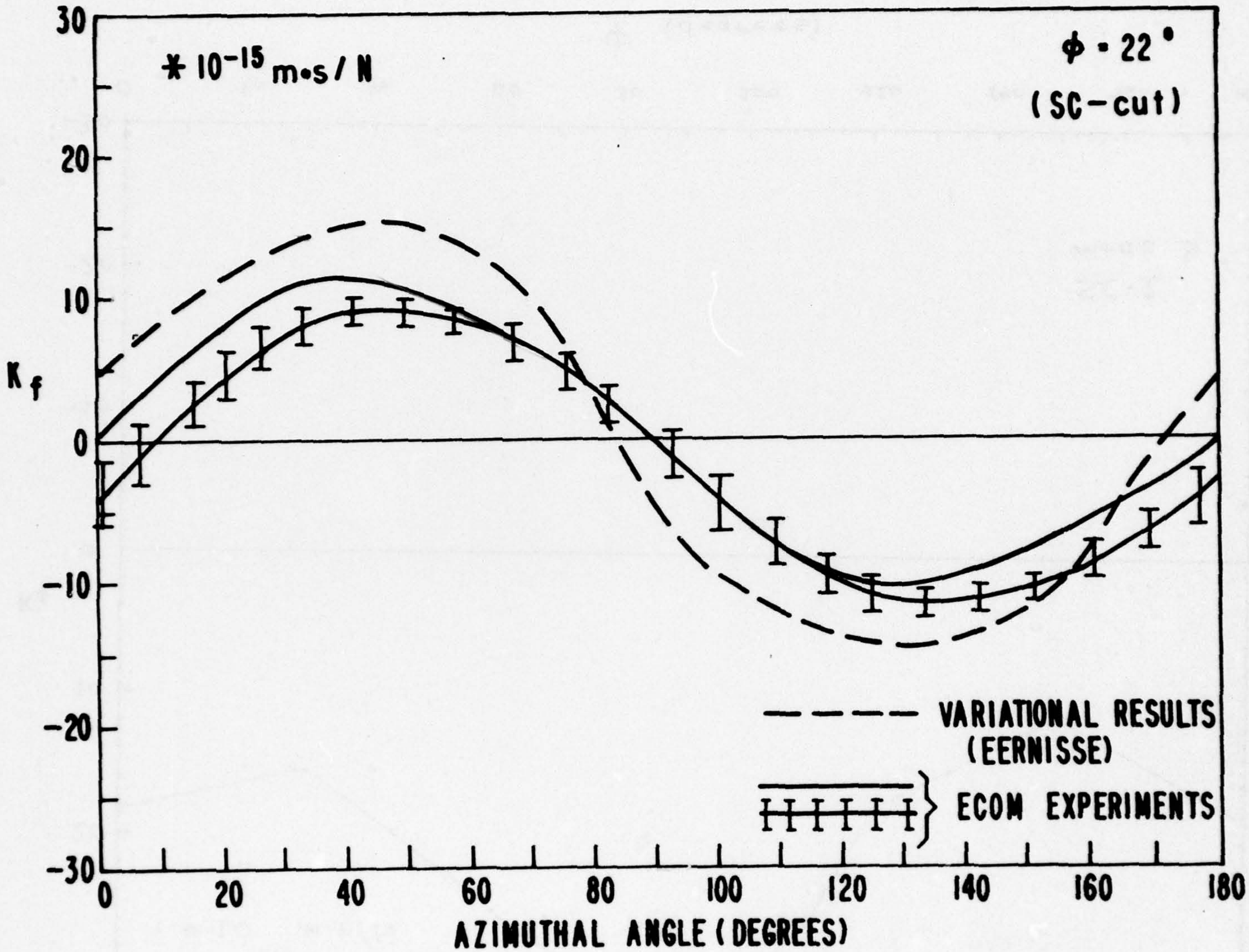


FIGURE 25. EXPERIMENTAL AND THEORETICAL RESULTS FOR PHI EQUALS 21.9 DEGREES.

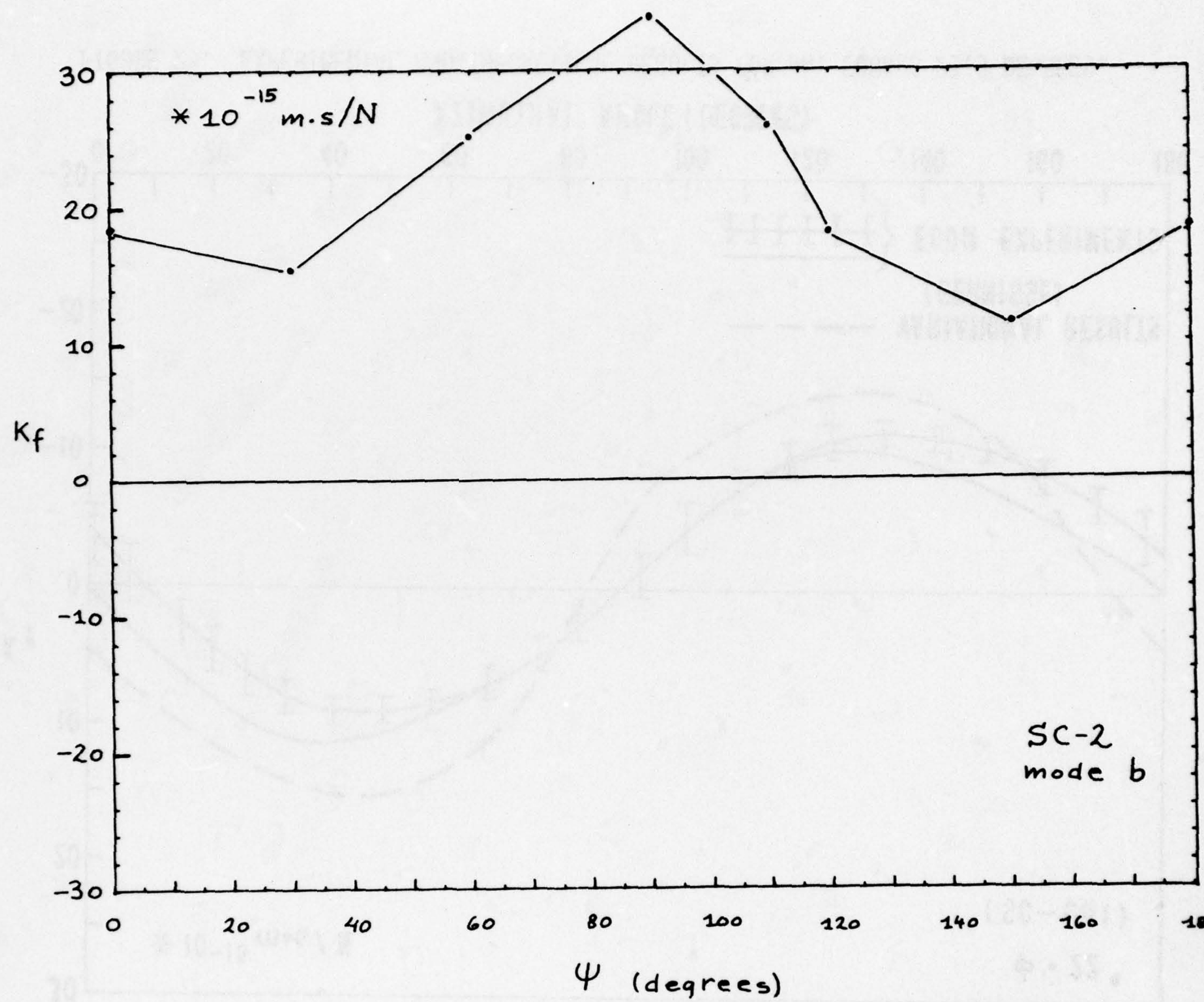


FIGURE 26. $K_F$ VERSUS PSI, MEASURED FOR THE SC-CUT B-MODE.

the large temperature coefficient, the force coefficient measurements are not as easy to make as for the c-mode. The results reported in Figure 26 should be regarded as tentative; they disclose, however, that $K_f$ exhibits no zeros along the $\psi$ axis.

## CONCLUSIONS

Doubly rotated quartz resonators have been considered as to frequency-temperature behavior, mode spectrum content, and primarily with respect to the force-frequency effect. It was found that the f-T curve shifts upward in temperature with increasing $\phi$ angle and becomes flatter. The mode spectrum is complicated by the presence of all three thickness modes, but their anharmonic overtones may be very adequately suppressed by means of energy trapping.

In the force-frequency portion, the calculus of variations has been used to obtain solutions for the static stress distributions caused in circular quartz resonator blanks by forces acting along a diameter. The resulting static stress distributions have been used to predict the force sensitivity of the resonant frequency of thickness shear resonators. The present results are shown to agree more favorably with experiment than results obtained by previous theories where the quartz was assumed to be isotropic for the static stress solution. General results are given by the doubly-rotated family (YXwℓ)$\phi/\theta$ along the technologically important zero temperature branch which contains the AT- , FC- , IT- , and SC-cuts. The results will be useful for choosing the location of bonding pads for two-point mounts so that mounting stress effects can be minimized.

## REFERENCES*

1. A. D. Ballato, "Effects of Initial Stress on Quartz Plates Vibrating in Thickness Modes," Proc. 14th AFCS, May-June 1960, pp. 89-114.

2. R. Holland, "Nonuniformly Heated Anisotropic Plates: II. Frequency Transients in AT and BT Quartz Plates," Proc. IEEE Ultrasonics Symposium, Nov. 1974, pp. 592-598.

3. E. P. EerNisse, "Quartz Resonator Frequency Shifts Arising from Electrode Stress," Proc. 29th AFCS, May 1975, pp. 1-4.

4. J. Kusters, "Transient Thermal Compensation for Quartz Resonators," IEEE Trans. Sonics Ultrason., Vol. SU-23, No. 4, July 1976, pp. 273-276.

5. E. P. EerNisse, "Calculations on the Stress Compensated (SC-Cut) Quartz Resonator," Proc. 30th AFCS, June 1976, pp. 8-11.

6. A. Ballato and G. J. Iafrate, "The Angular Dependence of Piezoelectric Plate Frequencies and Their Temperature Coefficients," Proc. 30th AFCS, June 1976, pp. 141-156.

7. R. Holland, "Temperature Coefficients of Stiffness in Quartz," IEEE Trans. Sonics Ultrason., Vol. SU-23, No. 1, Jan. 1976, pp. 72-75.

---

*AFCS: Annual Frequency Control Symposium, US Army Electronics Command, Fort Monmouth, NJ 07703.

8. J. A. Kusters and J. G. Leach, "Further Experimental Data on Stress and Thermal Gradient Compensated Crystals," Proc. IEEE, Vol. 65, No. 2, Feb. 1977, pp. 282-284.

9. J. A. Kusters, C. A. Adams, and H. Yoshida, "Thermal Transient Compensated Crystal Cuts--TTC's; Further Developmental Results," Proc. 31st AFCS, June 1977, in press.

10. J. -J. Gagnepain, J. C. Ponçot, and C. Pegeot, "Amplitude-Frequency Behavior of Doubly Rotated Quartz Resonators," Proc. 31st AFCS, June 1977, in press.

11. A. Ballato, E. P. EerNisse, and T. Lukaszek, "The Force-Frequency Effect in Doubly Rotated Quartz Resonators," Proc. 31st AFCS, June 1977, in press.

12. A. Ballato, "Temperature Compensated Crystal Oscillator (TCXO) Design Aids: Frequency-Temperature Resonator Characteristics as Shifted by Series Capacitors," Technical Report ECOM-4498, US Army Electronics Command, Fort Monmouth, NJ 07703, May 1977, 59 pp.

13. A. Ballato, "Doubly Rotated Thickness Mode Plate Vibrators," in Physical Acoustics: Principles and Methods, (W. P. Mason and R. N. Thurston, eds.), Vol. 13, Chap. 5. Academic Press, New York, 1977, pp. 115-181.

14. E. A. Gerber, "Precision Frequency Control for Guided Missiles," Proc. 1st IRE National Convention on Military Electronics, Session 6, June 1957, pp. 91-98.

15. E. A. Gerber, "Reduction of Frequency-Temperature Shift of Piezoelectric Crystals by Application of Temperature-Dependent Pressure," Proc. IRE, Vol 48, No. 2, February 1960, pp. 244-245.

16. A. D. Ballato and R. Bechmann, "Effect of Initial Stress in Vibrating Quartz Plates," Proc. IRE, Vol. 48, No. 2, February 1960, pp. 261-262.

17. E. A. Gerber and M. H. Miles, "Temperature Compensation of Piezoelectric Resonators by Mechanical Stress," Proc. 15th AFCS, May-June 1961, pp. 49-65.

18. E. A. Gerber and M. H. Miles, "Reduction of the Frequency-Temperature Shift of Piezoelectric Resonators by Mechanical Stress," Proc. IRE, Vol. 49, No. 11, November 1961, pp. 1650-1654.

19. R. W. Keyes and F. W. Blair, "Stress Dependence of the Frequency of Quartz Plates," Proc. IEEE, Vol. 55, No. 4, April 1967, pp. 565-566.

20. J. M. Ratajski, "Force-Frequency Coefficient of Singly-Rotated Vibrating Quartz Crystals," IBM J. Res. Dev., Vol. 12, No. 1, January 1968, pp. 92-99.

21. P. C. Y. Lee, Y. S. Wang, and X. Markenscoff, "Elastic Waves and Vibrations in Deformed Crystal Plates," Proc. 27th AFCS, June 1973, pp. 1-6.

22. P. C. Y. Lee, Y. S. Wang, and X. Markenscoff, "Effects of Initial Bending on the Resonance Frequencies of Crystal Plates," Proc. 28th AFCS, May 1974, pp. 14-18.

23. P. C. Y. Lee and D. W. Haines, "Piezoelectric Crystals and Electro-elasticity," in R. D. Mindlin and Applied Mechanics, (G. Herrmann, ed.) Pergamon Press, New York, 1974, pp. 227-253.

24. P. C. Y. Lee, Y. S. Wang, and X. Markenscoff, "High Frequency Vibrations of Crystal Plates under Initial Stresses," J. Acoust. Soc. Amer., Vol 57, No. 1, Jan 1975, pp. 95-105.

25. P. C. Y. Lee, Y. S. Wang, and X. Markenscoff, "Nonlinear Effects of Initial Bending on the Vibrations of Crystal Plates," J. Acoust. Soc. Am., Vol. 59, No. 1, Jan. 1976, pp. 90-96.

26. M. Valdois, J. Besson, and J. -J. Gagnepain, "Influence of Environment Conditions on a Quartz Resonator," Proc. 28th AFCS, May 1974, pp. 19-32.

27. P. C. Y. Lee and K. -M. Wu, "Effects of Acceleration on the Resonance Frequencies of Crystal Plates," Proc. 30th AFCS, June 1976, pp. 1-7.

28. D. Hammond, C. Adams, and L. Cutler, "Precision Crystal Units," Proc. 17th AFCS, May 1963, pp. 215-232.

29. J. -J. Gagnepain, "Mécanismes Non-Linéaires dans les Résonateurs à Quartz," Doctoral Thesis No. 59, Université de Besançon, March 1972.

30. H. F. Tiersten, "Analysis of Nonlinear Resonance in Rotated Y-Cut Quartz Thickness-Shear Resonators," Proc. 29th AFCS, May 1975, pp. 49-53.

31. H. F. Tiersten, "Analysis of Nonlinear Resonance in Thickness-Shear and Trapped-Energy Resonators," J. Acoust. Soc. Am., Vol. 59, No. 4, April 1976, pp. 866-878.

32. W. H. Horton and R. C. Smythe, "Experimental Investigations of Intermodulation in Monolithic Crystal Filters," Proc. 27th AFCS, June 1973, pp. 243-245.

33. R. C. Smythe, "Intermodulation in Thickness-Shear Resonators," Proc. 28th AFCS, May 1974, pp. 5-7.

34. H. F. Tiersten, "Analysis of Intermodulation in Rotated-Y-Cut Quartz Thickness-Shear Resonators," Proc. 28th AFCS, May 1974, pp. 1-4.

35. H. F. Tiersten, "Analysis of Intermodulation in Thickness-Shear and Trapped Energy Resonators," J. Acoust. Soc. Am., Vol. 57, No. 3, March 1975, pp. 667-681.

36. E. Hafner, "Some Phenomena in VHF Crystal Units," Proc. 10th AFCS, May 1956, pp. 182-189.

37. H. Fukuyo, H. Yoshie, and M. Nakazawa, "The Unwanted Responses of Crystal Oscillator Controlled by AT-Cut Plate," Bull. Tokyo Inst. Tech., No. 82, Sept. 1967, pp. 53-64; Proc. 21st AFCS, April 1967, pp. 402-419.

38. C. Franx, "On Activity Dips of AT Crystals at High Levels of Drive," Proc. 21st AFCS, April 1967, pp. 436-454.

39. A. F. B. Wood and A. Seed, "Activity Dips in AT-Cut Crystals," Proc. 21st AFCS, April 1967, pp. 420-435.

40. I. Koga, "Anomalous Vibrations in AT-Cut Plates," Proc. 23rd AFCS, May 1969, pp. 128-131.

41. J. Birch and D. A. Weston, "Frequency/Temperature, Activity/Temperature Anomalies in High Frequency Quartz Crystal Units," Proc. 30th AFCS, June 1976, pp. 32-39.

42. P. F. Godwin, Jr., and G. L. Snider, "Methods for Production Screening for Anamalous Responses in Quartz Crystals Intended for High Reliability Applications," Proc. 31st AFCS, June 1977, in press.

43. A. Ballato and R. Tilton, "Ovenless Activity Dip Tester," Proc. 31st AFCS, June 1977, in press.

44. R. L. Filler and J. R. Vig, "The Effect of Bonding on the Frequency vs. Temperature Characteristics of AT-Cut Resonators," Proc. 30th AFCS, June 1976, pp. 264-268.

45. E. Hafner, "Crystal Resonators," IEEE Trans. Sonics Ultrason., Vol. SU-21, No. 4, October 1974, pp. 220-237.

46. "Standards on Piezoelectric Crystals, 1949," Proc. IRE, Vol. 37, No. 12, December 1949, pp. 1378-1395. (IEEE Standard No. 176.)

47. W. Shockley, D. R. Curran, and D. J. Koneval, "Trapped-Energy Modes in Quartz Filter Crystals," J. Acoust. Soc. Amer., Vol. 41, No. 4 (Part 2), April 1967, pp. 981-993.

48. T. J. Lukaszek and H. P. Wasshausen, "New Design Information for Filter Crystals in the 3.9-10 Mc/s Frequency Range," Proc. IEEE, Vol. 53, No. 11, November 1965, P. 1772.

49. R. D. Mindlin, "Optimum Sizes and Shapes of Electrodes for Quartz Resonators," J. Acoust. Soc. Amer., Vol. 43, No. 6, June 1968, pp. 1329-1331.

50. G. Temple and W. G. Bickley, Rayleigh's Principle and Its Applications to Engineering, Dover, New York, 1956.

51. R. Holland and E. P. EerNisse, Design of Resonant Piezoelectric Devices, Research Monograph No. 56, M.I.T. Press, Cambridge, MA, 1969.

52. S. H. Gould, Variational Methods for Eigenvalue Problems, Univ. Toronto Press, Toronto, and Oxford Univ. Press, London, 1966.

53. H. J. McSkimin, P. Andreatch, Jr., and R. N. Thurston, "Elastic Moduli of Quartz versus Hydrostatic Pressure at 25° and -195.8°C," J. Appl. Phys., Vol. 36, No. 5, May 1965, pp. 1624-1632.

54. R. N. Thurston, H. J. McSkimin, and P. Andreatch, Jr., "Third-Order Elastic Coefficients of Quartz," J. Appl. Phys., Vol. 37, No. 1, Jan. 1966, pp. 267-275.

55. H. Goldstein, Classical Mechanics, Addison-Wesley, Reading, MA, and London, 1950.

56. S. Timoshenko and J. N. Goodier, Theory of Elasticity, McGraw-Hill, New York, 1951.

57. "Crystal Impedance Meter TS-330/TSM," Department of the Army Technical Manual TM 11-5051, Department of the Army, Washington, DC 20025, 4 April 1951, 71 pp.

## APPENDIX A

### RESONATOR PREPARATION

The resonator plates used for these investigations were of three orientations:

$$\phi = 10^\circ \ , \ \theta = 34^\circ 50'$$
$$15^\circ \qquad 34^\circ 16' \text{ (FC-cut)}$$
$$21.9^\circ \qquad 33^\circ 54' \text{ (SC-cut).}$$

Each orientation group consisted of four crystals. Initial thicknesses varied from $t_a = 0.635$ mm to 1.397 mm. All crystal blanks were rough-lapped to a thickness of 0.559 mm with #400 mesh silicon carbide in a water slurry. The plates were then reduced to the operating thickness according to the following schedule:

| Grit Size | Material Removed | Plate Thickness |
|---|---|---|
| # 600 | 0.076 mm | |
| | | 0.483 mm |
| 12 µm | 0.076 mm | |
| | | 0.407 mm |
| 5 µm | 0.051 mm | |
| | | 0.356 mm |
| 3 µm | 0.038 mm | |
| | | 0.318 mm |
| Polishing Compound (cerium oxide) | 0.013 mm | |
| | | 0.305 mm |

The final plate thickness brings the c-mode fundamental resonance into the neighborhood of 6 MHz.

In the lapping process, the crystals were grouped according to orientation and thicknesses to within $\pm 0.013$ mm for each of the above stages. These groups, in turn, were cemented with a wax-rosin compound to a 75 mm diameter optical flat (flatness better than $\lambda_{Hg}/10$) during lapping as a means of assuring orientational integrity and parallelism.

All blanks were rounded after lapping. The plates were loafed together in standard fashion, and the diameter reduced to 14.18 mm for the SC-cut units and 13.97 mm for the $\phi = 10^\circ$ and $15^\circ$ cuts. The final diameter was reached when, upon microscopic inspection, all hairline cracks, chips, and scratches were removed.

The cleaning procedure consisted in washing the blanks in detergent and rinsing them under running tap water, as a first step. (Cleaning was limited to this first step in the washings that took place between successive stages of the lapping procedure discussed above, and during each reversal of the plates on the optical flat.)

Cleaning of the polished resonator blanks prior to electrode plating consisted of the further steps:

- Inserting blanks into specially constructed stainless steel wire jigs.
- Degreasing in boiling acetone or methanol for 3 minutes.
- Rinsing in hot distilled water in two successive stages.
- Agitating in ultrasonic bath with hot ethyl alcohol for 1 or 2 minutes.
- Blowing dry with hot air (blanks still in jig).

After the cleaning, the blanks were removed from the holder jig by teflon-coated tweezer and placed in a UV/ozone cleaning facility. This has been shown to be an effective way of removing a variety of contaminants from quartz surfaces.[1,2]

The blanks were electroded with argon-sputtered gold films to a diameter of 5 mm with a connecting tab in a keyhole pattern. Plateback values were as follows:

$$\begin{array}{ll} \mu = 0.8\% \quad , & \phi = 10^\circ \\ \phantom{\mu = {}}1.3\% & \phantom{\phi = {}}15^\circ \\ \phantom{\mu = {}}1.8\% & \phantom{\phi = {}}21.9^\circ \end{array}$$

Excitation of these plates was made possible by bonding 0.127 mm wires directly to the electrode tabs with electrically-conducting cement.

---

1. J. R. Vig, C. F. Cook, Jr., K. Schwidtal, J. W. LeBus, and E. Hafner, "Surface Studies for Quartz Resonators," Proc. 28th AFCS,* May 1974, pp. 96-108.

2. J. R. Vig, J. W. LeBus, and R. L. Filler, "Further Results on UV Cleaning and Ni Electrobonding," Proc. 29th AFCS, May 1975, pp. 220-229.

*AFCS: Annual Frequency Control Symposium, US Army Electronics Command, Fort Monmouth, NJ 07703.

DEPARTMENT OF THE ARMY
HEADQUARTERS
UNITED STATES ARMY ELECTRONICS COMMAND
FORT MONMOUTH, NEW JERSEY 07703
ATTN DRSEL-MS-TI
OFFICIAL BUSINESS

POSTAGE AND FEES PAID
DEPARTMENT OF THE ARMY
DOD-314